

1 **Vegetation-climate feedbacks modulate rainfall patterns in Africa under**  
2 **future climate change**

3 M. Wu<sup>1</sup>, G. Schurgers<sup>2</sup>, M. Rummukainen<sup>1,3</sup>, B. Smith<sup>1</sup>, P. Samuelsson<sup>4</sup>, C. Jansson<sup>4</sup>, J.  
4 Siltberg<sup>1</sup>, W. May<sup>3,5</sup>

5 [1]{Department of Physical Geography and Ecosystem Science, Lund University, Sölvegatan 12, SE-  
6 223 62, Lund, Sweden}

7 [2]{Department of Geosciences and Natural Resource Management, University of Copenhagen,  
8 Øster Voldgade 10, DK-1350 Copenhagen, Denmark}

9 [3]{Centre for Environmental and Climate Research, Lund University, Sölvegatan 37, SE-223 62 Lund,  
10 Sweden}

11 [4]{Rosby Centre, Swedish Meteorological and Hydrological Institute, SE-601 76, Norrköping,  
12 Sweden}

13 [5]{Research and Development Department, Danish Meteorological Institute, Lyngbyvej 100, DK-  
14 2100 Copenhagen, Denmark}

15

16

17 Correspondence to: M. Wu (minchao.wu@nateko.lu.se)

18

19

20

21

22

23

24

25

26

27

28

29

30 ***Abstract***

31 Africa has been undergoing significant changes in climate and vegetation in recent decades,  
32 and continued changes may be expected over this century. Vegetation cover and  
33 composition impose important influences on the regional climate in Africa. Climate-driven  
34 changes in vegetation structure and the distribution of forests versus savannah and  
35 grassland may feed back to climate via shifts in the surface energy balance, hydrological  
36 cycle and resultant effects on surface pressure and larger-scale atmospheric circulation. We  
37 used a regional Earth system model incorporating interactive vegetation-atmosphere  
38 coupling to investigate the potential role of vegetation-mediated biophysical feedbacks on  
39 climate dynamics in Africa in an RCP8.5-based future climate scenario. The model was  
40 applied at high resolution (0.44 x 0.44 degrees) for the CORDEX-Africa domain with  
41 boundary conditions from the CanESM2 GCM. We found that increased tree cover and leaf-  
42 area index (LAI) associated with a CO<sub>2</sub> and climate-driven increase in net primary  
43 productivity, particularly over sub-tropical savannah areas, not only imposed important local  
44 effect on the regional climate by altering surface energy fluxes, but also resulted in remote  
45 effects over central Africa by modulating the land-ocean temperature contrast, Atlantic  
46 Walker circulation and moisture inflow feeding the central African tropical rainforest region  
47 with precipitation. The vegetation-mediated feedbacks were in general negative with  
48 respect to temperature, dampening the warming trend simulated in the absence of  
49 feedbacks, and positive with respect to precipitation, enhancing rainfall reduction over the  
50 rainforest areas. Our results highlight the importance of accounting for vegetation-  
51 atmosphere interactions in climate projections for tropical and sub-tropical Africa.

52

53        **Keywords:** RCA-GUESS, Vegetation Dynamics, Biophysical feedback, Precipitation,  
54 Walker Circulation, Land-ocean Contrast, Regional Climate Model

55

56

57

58

59

60

61

62

63

64

65

66

67

68

69

70

71

72

73

74

75

76

77

78

## 79 **1. Introduction**

80 The Sahel greening and Congo rainforest browning observed since the 1980s suggest that  
81 Africa has been undergoing significant changes in the structure, composition and  
82 distribution of vegetation during recent decades (Eklundh and Olsson, 2003;Olsson et al.,  
83 2005;Jamali et al., 2014;Zhou et al., 2014). In addition to influences from anthropogenic  
84 activity (e.g. changes in land use), vegetation changes in the region have been linked to  
85 changes in recorded climatic conditions, including the trend and interannual variability of  
86 precipitation (Herrmann et al., 2005;Hickler et al., 2005;Olsson et al., 2005;Zhou et al., 2014),  
87 which in turn have been related to decadal-scale changes in regional circulation (Camberlin  
88 et al., 2001;Giannini et al., 2003). On longer timescales, anthropogenic climate change has  
89 the potential to cause profound structural and compositional changes in vegetation over  
90 Africa (Sitch et al., 2008;Scheiter and Higgins, 2009).

91 Shifts in vegetation cover and composition in terms of the distribution of trees and  
92 grasses and their seasonal changes (phenology) can impose significant forcings on the  
93 physical climate system by modulating surface-atmosphere energy exchange and  
94 hydrological cycling, resulting in biophysical feedbacks along with the climate forcings. The  
95 type of vegetation alongside productivity-related structural aspects such as tree density and  
96 leaf area index (LAI) are important determinants for surface albedo, roughness length and  
97 evapotranspiration, affecting surface energy fluxes that in turn control lower boundary layer  
98 thermodynamics (Eltahir, 1996;Brovkin et al., 2006;Bonan, 2008). Biophysical feedbacks  
99 operate locally and may also generate teleconnections via heat and moisture advection,  
100 leading to altered atmospheric circulation (e.g. Avissar and Werth, 2005;Nogherotto et al.,  
101 2013). Previous studies have shown the importance of vegetation-mediated biophysical

102 feedbacks for the past (e.g. Claussen and Gayler, 1997;Texier et al., 1997), and present (e.g.  
103 Eltahir, 1996;Claussen, 1998;Wang and Eltahir, 2000) climate over Africa. Hypothesised  
104 mechanisms of vegetation-atmosphere coupling include modulations of the surface albedo  
105 (Charney, 1975), changes in the North-African monsoon system (Claussen, 1997) and  
106 internal climate variability (Zeng et al., 1999).

107       Feedbacks mediated by shifts in vegetation structure and distribution can likewise play a  
108 role for the future regional climate. General circulation models (GCMs) have been applied at  
109 relatively coarse lateral grid resolutions to capture these dynamics (e.g. Kucharski et al.,  
110 2013). Recent studies have used a regional climate model to investigate the impact of  
111 climate-vegetation interaction for West Africa, identifying significant vegetation feedback in  
112 modulating local hydrological cycling (e.g. Alo and Wang, 2010;Wang and Alo, 2012;Yu et al.,  
113 2015). Additionally, a number of GCM-based studies have investigated the climate effects of  
114 anthropogenic perturbations, such as deforestation or afforestation (e.g. Lawrence and  
115 Vandecar, 2015). Such studies point to potentially significant forcing of regional climate  
116 dynamics, particularly rainfall patterns, as a result of changes in land cover. No study to date  
117 has, however, characterised the coupled dynamics of vegetation and climate under future  
118 radiative forcing for the entire African domain at a grid resolution high enough to capture  
119 regional features and forcings.

120       In this study, we employ a regional Earth system model (ESM) that couples the physical  
121 component of a regional climate model (RCM) with a detailed, individual-based dynamic  
122 vegetation model (DVM). This tool enables dynamic representation of biophysical  
123 interactions between the vegetated land surface and the atmosphere and their effects on  
124 the evolution of climate and land surface biophysical properties to be analysed in an explicit

125 way. We perform simulations under the Representative Concentration Pathway (RCP) 8.5  
126 radiative forcing scenario (Moss et al., 2010) with and without vegetation feedbacks  
127 enabled, and investigate the potential coupled evolution of climate and vegetation for the  
128 African continent over the 21<sup>st</sup> century. Our focus is especially on the central African  
129 rainforest areas and the surrounding savannah vegetation belt.

## 130 ***2. Data and Method***

### 131 ***2.1 Model description***

132 RCA-GUESS (Smith et al., 2011) is a regional ESM based on the Rossby Centre regional  
133 climate model RCA4 (Kjellström et al., 2005;Samuelsson et al., 2011) coupled with  
134 vegetation dynamics from the LPJ-GUESS DVM to account for land-atmosphere biophysical  
135 coupling (Smith et al., 2001;Smith et al., 2014).

136 The RCA4-based physical component of RCA-GUESS incorporates advanced regional surface  
137 heterogeneity, such as complex topography and multi-level representations for forests and  
138 lakes, which are significant in controlling the development of weather events from the local-  
139 to meso-scale (Samuelsson et al., 2011). RCA4 has been applied in a range of climate  
140 studies worldwide (e.g., Döscher et al., 2010;Kjellström et al., 2011;Sörensson and  
141 Menéndez, 2011). The land surface scheme (LSS, Samuelsson et al., 2006) adopts a tile  
142 approach and characterizes land surface with open land and forest tiles with separate  
143 energy balances. The open land tile is divided into fractions for vegetation (herbaceous  
144 vegetation) and bare soil. The forest tile is vertically divided into three sub-levels (canopy,  
145 forest floor and soil). Surface properties such as surface temperature, humidity and  
146 turbulent heat fluxes (latent and sensible heat fluxes) for different tiles in a grid box are

147 weighted together to provide grid-averaged values. A detailed description is given by  
148 Samuelsson et al. (2006).

149 The vegetation dynamics component of RCA-GUESS employs a plant individual and patch-  
150 based representation of the vegetated landscape, optimized for studies at regional and  
151 global scale. Heterogeneities of vegetation structure and their effects on ecosystem  
152 functions such as carbon and water vapour exchange with the atmosphere are represented  
153 dynamically, affected by allometric growth of age-size classes of woody plant individuals,  
154 along with a grass understorey, and their interactions in competition for light and soil  
155 resources. Plant functional types (PFTs) encapsulate the differential functional responses of  
156 potentially-occurring species in terms of growth form, bioclimatic distribution, phenology,  
157 physiology and life-history characteristics. Multiple patches in each vegetated tile account  
158 for the effects of stochastic disturbances, establishment and mortality on local stand history  
159 (Smith et al., 2001). This explicit, dynamic representation of vertical structure and landscape  
160 heterogeneity of vegetation has been shown to result in realistic simulated vegetation  
161 dynamics in numerous studies using the offline LPJ-GUESS model (Smith et al., 2001;Weber  
162 et al., 2009;Hickler et al., 2012;Smith et al., 2014;Wårlind et al., 2014;Wu et al., 2015).

163 Biophysical feedbacks have previously been studied in applications of RCA-GUESS to Europe  
164 and the Arctic (Wramneby et al., 2010;Smith et al., 2011;Zhang et al., 2014). A general  
165 description of the coupling between the vegetation dynamics component LPJ-GUESS and  
166 the physical component RCA is provided in the Appendix. A more detailed description is  
167 given by Smith et al. (2011).

## 168 **2.2 Model setup, experiments and analysis approach**

169 The simulations were applied over the African domain of the Coordinated Regional Climate  
170 Downscaling Experiment (CORDEX-Africa, Giorgi et al., 2009; Jones et al., 2011) on a  
171 horizontal grid with a resolution of  $0.44^\circ \times 0.44^\circ$ . The period studied was 1961 to 2100.  
172 Forcing fields in 6-hour time intervals (atmospheric fields and sea-surface temperature (SST)  
173 as lateral and lower boundary conditions, respectively) were derived from the historical and  
174 RCP8.5 simulations with the CanESM2 general circulation model (GCM) (Arora et al., 2011)  
175 in the Coupled Model Intercomparison Project Phase 5 (CMIP5, Taylor et al., 2012). Time-  
176 evolving forcing fields from the GCM were prescribed for all variables, including SSTs.

177 The vegetation sub-model LPJ-GUESS was set up with eight PFTs which represent the major  
178 elements of natural vegetation across Africa, including the tropical and warm-temperate  
179 forests and savannahs and  $C_3$  and  $C_4$  grasslands. The PFT parameter settings follow Morales  
180 et al. (2007) and are summarised in Table A1.

181 PFTs of the forest tile were simulated with 30 replicate patches. Average values of state  
182 variables across the replicate patches were used to determine biophysical parameters, i.e.  
183 forest fraction and LAI for trees versus grasses, provided as forcing to the physical sub-  
184 model. For the open land tile with herbaceous species,  $C_3$  and  $C_4$  grass were simulated  
185 deterministically and aggregated to characterise open land vegetation. Fire disturbance in  
186 response to climate and simulated fuel load (Thonicke et al., 2001) was included.

187 Following the approach of Wramneby et al. (2010) and Smith et al. (2011), RCA-GUESS was  
188 initialized with a spin-up in two stages to achieve a quasi-steady state representative for  
189 mid-1900's conditions. After the spin-up, the model was run in coupled mode from 1961  
190 onwards, with simulated meteorological forcing from the physical sub-model affecting  
191 vegetation phenology and structural dynamics, and biophysical land surface properties



192 being adjusted to reflect the changes in vegetation, thereby affecting the physical climate  
193 dynamics. For comparison, a recent past experiment (RP, Table 1) with the same vegetation  
194 spin-up but thereafter driven by boundary conditions derived from ECMWF re-analysis (ERA-  
195 Interim) (Berrisford et al., 2009), was conducted for the period 1979-2011.

196 The simulation protocol was designed to enable biophysical feedbacks of vegetation  
197 changes to the evolving 21st century climate to be inferred. Three simulations were  
198 performed to investigate vegetation-climate feedbacks under future climate change (Table  
199 1). The first simulation included the vegetation feedback (FB). It was run for 1961-2100 in  
200 coupled mode, allowing the effects of climate and atmospheric CO<sub>2</sub> concentration (the  
201 latter taken directly from the RCP 8.5 data set) on vegetation state to feed back to the  
202 evolving climate. The second simulation was run with vegetation feedback “switched off”  
203 (non-feedback run, NFB). It started with the state of FB simulation at 1991 and used a  
204 prescribed climatology of daily vegetation for 1961-1990 from the coupled simulation, but  
205 without transferring the simulated changes in vegetation in LPJ-GUESS to the land surface  
206 configuration, and associated biophysical surface properties, in the LSS of RCA. To attribute  
207 the component of the simulated vegetation changes resulting from physiological effects of  
208 rising CO<sub>2</sub> concentrations of plant productivity and water-use efficiency, we performed a  
209 third simulation (FB\_CC), which was similar to FB, but started from the state of the FB  
210 simulation of 1991 and used historical atmospheric CO<sub>2</sub> concentrations until 2005, held  
211 constant thereafter, to force the vegetation sub-model only.

212 Our analysis focuses on the future period 2081-2100, comparing this with the present-day  
213 (1991-2010). The climate change signal is inferred from the difference between the future

214 mean and the present-day mean in the NFB run. Vegetation feedbacks are calculated as the  
215 difference between the future means of the FB and NFB runs.

## 216 **2.3 Methods to evaluate model performance**

217 Simulated near-surface atmospheric temperature over open land, precipitation, and LAI  
218 were compared against observations within the common available time period 1997-2010.  
219 Temperature and precipitation were compared with gridded observations from the CRU  
220 TS3.23 (Harris et al., 2014) dataset, focusing on the annual mean and seasonality. For  
221 precipitation we also employed the GPCP (Huffman et al., 2001, version 1.2 of One-Degree  
222 Daily product for 1996/10-2011/6) which uses satellite data to upscale rain gauge  
223 measurements and has been extensively used for African precipitation studies (e.g., Nikulin  
224 et al., 2012). For the LAI evaluation we used the GIMMS-AVHRR and MODIS-based LAI3g  
225 product (Zhu et al., 2013) which has been previously applied to the evaluation of vegetation  
226 dynamics in ESMs (e.g., Anav et al., 2013).

227 To identify biases propagating from the model physics and from the GCM-derived boundary  
228 forcing data, we compared the reanalysis-driven RP simulation against observation and  
229 against the GCM-driven (CanESM2) FB simulation for the same period.

## 230 **3. Results**

### 231 **3.1 Model evaluation**

232 To evaluate the model's performance for the present day, the simulated annual mean and  
233 seasonality of 2-meter air temperature, precipitation and LAI are compared against the  
234 observations (Fig. 1 and Fig. 2). The simulated annual mean temperature (Fig. 1a1) is  
235 generally higher in northern-hemisphere (hereinafter "northern") Africa than in southern-

236 hemisphere (hereinafter “southern”) Africa. The model generally shows a cold bias in the  
237 order of 1°C for northern and southern savannah (Fig. 1a2), dominated by the northern  
238 hemisphere summer (JJA, Fig. 2a1,2a3). Warm biases up to around 3°C occur in northern  
239 Africa, and warm biases up to around 1°C in central Africa where the warm bias originates  
240 mainly from summer (Fig. 2a2).

241 The simulated precipitation is largest over western and central Africa up to 1600 mm  
242 year<sup>-1</sup> within the simulated rainbelt between 25°N and 25°S, where the Atlantic moisture  
243 inflow (monsoon and equatorial westerlies) plays an important role (Fig. 1b1). Comparison  
244 with CRU reveals a considerable dry bias (-500 mm year<sup>-1</sup>) for the central African rainforest  
245 area and a wet bias (+250 mm year<sup>-1</sup>) for the northern savannah. The simulated patterns and  
246 magnitude of precipitation for this area are similar to a previous study using an earlier  
247 version of RCA, RCA3.5, without dynamic vegetation (Nikulin et al., 2012). In RCA, the dry  
248 bias for annual mean precipitation over central Africa may be partly due to the  
249 underestimated daily precipitation during the late afternoon and night in addition to  
250 observational uncertainties (Nikulin et al., 2012). The wet bias over the northern savannah is  
251 mainly caused by a too early onset of the rainy season (b1, Fig. 2), which is possibly caused  
252 by the interactions between the simulated deep convection and the Africa Easterly Waves  
253 (Sylla et al., 2011). The biases in simulated precipitation for the savannah regions and the  
254 central African rainforest area mirror the temperature biases: warm biases coincide with dry  
255 biases in central Africa, and cold biases coincide with wet biases in savannah regions. A  
256 comparison of the CanESM2-driven (FB run) and the ERA-Interim-driven (RP run) simulations  
257 (Fig. 1b3) indicates that the bias in simulated precipitation has contributions both from the  
258 RCM itself and from the GCM-generated boundary conditions. Nevertheless, Nikulin et al.

259 (2012) have previously shown for Africa that the model is able to capture the ITCZ position  
260 and the main features of the seasonal mean rainfall distribution and its annual cycle, and  
261 the model biases in precipitation were of similar magnitude to the differences between  
262 observational datasets.

263 To further diagnose the effect of model dynamics on the precipitation bias, we evaluated  
264 the low-level circulation and humidity, which play an important role in the moisture  
265 transport between ocean and land(Nicholson and Grist, 2003). The SST forcing is also  
266 important for the African climate, and the CanESM2 SSTs have been validated and shown to  
267 be accurate in previous studies (e.g. Rowell, 2013;LaRow et al., 2014;Xu et al., 2014). We  
268 compare the simulated circulation and specific humidity at 850 hPa from the NFB run with  
269 the regional model against ERA-Interim reanalysis for 1997-2010 (Fig. A1). The simulated  
270 patterns of circulation and specific humidity at 850 hPa agree well with the reanalysis: the  
271 trade winds over both northern and southern Atlantic, West African monsoon as well as the  
272 Somali Jet (eastern Africa) are reproduced well by the model. However, there are small  
273 biases in wind speed at 850 hPa which generally appear in areas close to the domain  
274 boundary and around the African coastal regions. In the case of specific humidity, there are  
275 dry biases over the continent. These may be traceable to the different convective schemes  
276 used in RCA and ERA-Interim, exhibiting different diurnal cycle of precipitation over Africa  
277 (Nikulin et al., 2012).

278 The simulated seasonality of LAI generally reflects the simulated seasonality of precipitation.  
279 A systematic overestimation is apparent for savannahs, and a significant underestimation  
280 for the central Africa rainforest area. These biases in LAI predominantly reflect the  
281 corresponding biases in precipitation (Fig. 2 b1-b3 and 2c1-c3). A stronger LAI bias in the

282 savannah is due to the presence of grasses, which are more sensitive to precipitation  
283 changes in the model compared to trees.

284 With present-day forcing, the simulated climate and vegetation patterns and phenology are  
285 generally consistent with observations. Some of the biases in the simulated climate are  
286 common to many RCMs (Nikulin et al., 2012) and they are apparent for some sub-regions  
287 and seasons in our model. We conclude that the performance is adequate to capture the  
288 main details of the African climatology, providing sufficient confidence for the subsequent  
289 analysis of regional vegetation-climate interactions under future climate change.

### 290 ***3.2 Future climate and vegetation change***

291 In the NFB simulation, most of the African continent is simulated to be 4-6°C warmer by the  
292 end of the 21<sup>st</sup> century compared with present day (Fig. 3a). The subtropics exhibit a slightly  
293 stronger warming than the tropics, and land warming is slightly larger compared to warming  
294 of the surrounding ocean surface as simulated by the CanESM2 GCM and represented in the  
295 SST forcing fields prescribed from that model. These changes are fairly similar throughout  
296 the year, except in Northern Africa and the Sahara, where the temperature increase is  
297 particularly pronounced in the local dry season (Fig. A2.e-h). Precipitation is projected to  
298 increase in most parts of the African monsoon area, western equatorial coastal area and the  
299 eastern African horn (Fig. A3.e-h). A slight decrease is projected in the Congo basin and for  
300 the southern part of the continent (Fig. 3c). For areas with a precipitation increase, the  
301 increase is mainly confined to the local wet season. The precipitation decrease over central  
302 and southern Africa is apparent throughout the year (Fig. A3.e-h).

303 Vegetation feedbacks (FB run) modify significantly the pattern and magnitude of simulated

304 climate change. The effects are largest in low-latitude areas where the surface temperature  
305 increase is generally dampened (negative feedback), most notably in savannah areas and to  
306 a lesser extent in the equatorial rainforest area (Fig. 3b). The precipitation decrease is  
307 enhanced (positive feedback), most notably over the rainforest area (Fig. 3d).

308 With the effects of climate change and CO<sub>2</sub> fertilization, future vegetation growth depicts an  
309 enhancement not only of vegetation productivity in general, but also of tree cover in  
310 subtropical savannah areas (Fig. 4a), displacing grasses and reflecting an increase in tree LAI  
311 of 0.5-2.4 during the growing season (Fig. 4b). This increase in tree cover reflects a general  
312 rise in vegetation productivity driven by rising atmospheric CO<sub>2</sub> concentrations on  
313 photosynthesis and water-use efficiency (Long, 1991;Hickler et al., 2008;Keenan et al.,  
314 2013). Results from the FB\_CC experiment in which CO<sub>2</sub> fertilisation was disabled reveal that  
315 changes in climate drivers alone are simulated to have minor or opposing effects on tree  
316 productivity and LAI due to reduced water availability (Fig. A4.), and that the changes seen in  
317 tree cover and LAI in the FB run hence originate primarily from CO<sub>2</sub> fertilization.

318 Temperature feedbacks tend to be strong in areas of increased tree cover (Fig. 3b, Fig. 4a).  
319 The cooling effects from vegetation feedbacks are strong (approximately -2°C) throughout  
320 the year, with the most pronounced cooling occurring in the local dry season (Fig. A2.i-l),  
321 when the newly established tree (with larger root depth than grass) transpires water that is  
322 taken up from the deeper soil layer. Transpiration from present-day grass is constrained by  
323 the low moisture levels in the top soil layer. As a result, the evaporative cooling effect  
324 becomes stronger when forest replaces open land. In the central African rainforest area,  
325 where an increase in LAI of about 0.5-1 is simulated in FB run compared with the NFB run,  
326 vegetation feedbacks on temperature are much smaller in the rainy season, but cause

327 cooling in the dry season.

328 Vegetation feedbacks on precipitation are also pronounced. For the southern hemisphere  
329 savannah area, a slight increase in precipitation (approximately 10%, Fig. 3d) was simulated,  
330 which is caused by strengthened convective activity (which coincides with enhanced  
331 radiation and latent heat fluxes) in the rainy season (DJF, Fig. A3.). This can be considered as  
332 a local effect of tree LAI increase. However, changes in precipitation are not restricted only  
333 to the areas where tree cover increases (Fig. 3d, Fig. 4a), which is suggestive of remote  
334 effects on tropical precipitation. This is further investigated in the sections below.

### 335 ***3.3 Vegetation feedback effects on circulation and precipitation***

336 Vegetation feedbacks on temperature in our simulations operate mainly via an increased  
337 surface area for evaporation and a stronger coupling to the atmosphere as tree cover, root  
338 depth and LAI increase relative to grasses, most notably in savannah areas, resulting in a  
339 shift of the evaporative fraction (ratio of latent heat flux to turbulent heat fluxes) and an  
340 increase in surface roughness length. Overall, the turbulent heat fluxes increase, which  
341 tends to cool the surface and the lower atmosphere, exceeding the opposing (warming)  
342 effects of increased vegetation cover on albedo, thus resulting in an overall cooling effect.  
343 Similar behaviour was seen in southern Europe in a previous study with RCA-GUESS  
344 (Wramneby et al., 2010).

345 The variability of precipitation over Africa is greatly influenced by the moisture advection  
346 from the ocean to land. Previous studies have noted on the influence of Atlantic Walker  
347 circulation on central African precipitation, as well as the role of the west African monsoon  
348 for precipitation over western Africa (e.g. Nicholson and Grist, 2003;Dezfuli and Nicholson,

2013; Pokam et al., 2014). These circulation systems are associated with thermal contrasts between ocean and land, creating a pressure contrast that tends to promote the movement of moist surface air from the Atlantic over land. We examined the land-ocean thermal contrast ( $\nabla T$ ) and geopotential contrast ( $\nabla \phi$ ) between the equatorial Atlantic and the near-coast African continent for three pressure levels between 850 hPa and 975 hPa, to characterise the circulation in the lower troposphere. We found that changes in  $\nabla T$  and  $\nabla \phi$  are highly inter-annually anti-correlated for the rainy seasons MAM and SON ( $r=-0.82$  and  $-0.64$ , respectively, Fig. 5; Fig. A5). The sensitivity of  $\nabla \phi$  to  $\nabla T$ , depicted as the slope in Fig. 5, is generally maintained in the future, with a slight decrease in the sensitivity for DJF and a slight increase for MAM.

Under the NFB future simulation, ocean-land contrast becomes larger (the absolute value of  $\nabla T$  increases by about  $0.5-1^\circ\text{C}$ , Table A2) as land temperature increases more than the GCM-simulated increase in SSTs provided as forcing to the regional model (Fig. A2.). Differential changes in features of the surface and lower atmosphere, such as changes in land-ocean contrasts in boundary layer lapse rate (Joshi et al., 2008) and changes in Bowen ratio over land (Sutton et al., 2007) explain such divergence in temperatures between ocean and land. As a result, except for SON,  $\nabla \phi$  is generally simulated to increase in the course of the simulation (Fig. A5), with the largest shift occurring in MAM ( $11.96 \text{ m}^2 \text{ s}^{-2}$  by the end of 21<sup>st</sup> century, Table A2). For SON,  $\nabla T$  increases but  $\nabla \phi$  does not, suggesting that the trend of  $\nabla \phi$  under climate change is associated with the GCM-derived boundary conditions, despite the strong regional coupling with  $\nabla T$  in terms of variability (Fig. A5).

In contrast, the increase in the  $\nabla T$  is dampened considerably when incorporating interactive vegetation. The resulting reduction in  $\nabla T$  offsets  $\nabla \phi$  uniformly and statistically significantly



372 for all seasons, generally counteracting the climate change effect on  $\nabla\phi$  (Fig. 5, Table A2).

### 373 **3.4 *Effects on Walker circulation and low-latitude precipitation***

374 The low-level equatorial westerlies are important to the central African rainfall. They are  
375 associated with the lower branch of the Walker cell located near the western equatorial  
376 coast of Africa, and they transfer moisture from the adjacent Atlantic to the eastern  
377 equatorial coast and the Congo basin (e.g. Nicholson and Grist, 2003;Schefuß et al.,  
378 2005;Cook and Vizy, 2015). These westerlies occur from March to October, being best  
379 developed in JJA. They shift northward with the excursion of the Inter Tropical Convergence  
380 Zone (ITCZ) and under the strong influence of the South Atlantic high pressure cell  
381 (Nicholson and Grist, 2003). This pattern is simulated by RCA-GUESS for the present-day  
382 climate (Fig. 6). Via this circulation system, moisture can reach far over the African landmass  
383 at around 28°E, upwell and integrate into the mid-level African Easterly Jet (AEJ) (Camberlin  
384 et al., 2001;Nicholson and Grist, 2003). RCA-GUESS reproduces this pattern with a realistic  
385 magnitude (Fig. 6, Fig. 7, Fig. 8, Fig. 9) when compared with previous studies based on  
386 reanalysis data (Camberlin et al., 2001;Nicholson and Grist, 2003).

387 In the NFB future simulation, equatorial westerlies are strengthened throughout the year  
388 both over ocean (Fig. 6) and over land (Fig. 7). Changes in wind speed ( $\Delta u$ ) can be explained  
389 by changes in the low-level pressure contrast between land and ocean (sect. 3.3), where  
390 strengthened  $\nabla\phi$  leads to enhanced  $u$ , especially for MAM when the zonal pressure contrast  
391 prevails (Table A2). Atmospheric specific humidity in the lower troposphere near the equator  
392 also increases by around 10%-20% for MAM and SON, extending from the ocean to inland  
393 along the equator (Fig. 8cd; Fig. 9cd). Meanwhile, changes in future rainfall are apparent

394 along the equator, with increases over the equatorial coastal or inland areas (Fig. A3.),  
395 concurrent with stronger moisture inflow to land in the low-level troposphere (Fig. 8cd; Fig.  
396 9cd).

397 Vegetation feedbacks are simulated to weaken the climate change enhancement of the  
398 Walker circulation, resulting in a weakening of the equatorial westerlies and counteracting  
399 the effects of climate change alone (Fig. 6i-l and Fig. 7i-l; Fig. 8ef and Fig. 9ef). These changes  
400 correspond well to changes in low-level ocean-land geopotential contrast  $\Delta\nabla\phi$  with the  
401 biggest impact for MAM and SON (Table A2). The weakened Walker circulation is also  
402 represented as suppressed vertical uplifting motions over central Africa (Fig. 8f and Fig. 9f).  
403 Atmospheric specific humidity at 850 hPa is reduced by approximately 7% due to vegetation  
404 feedbacks which are comparable to the contribution of climate change (Fig. 8ef vs. Fig. 8cd;  
405 Fig. 9ef vs. Fig. 9cd).

406 Analysis of the moisture flux convergence also confirms the impacts of a weakened Walker  
407 circulation (Fig. 10) on the hydrological cycle caused by vegetation feedback. Moisture fluxes  
408 for most parts of the African continent diverge toward the ocean near the equatorial  
409 regions. This divergence is similar for both MAM and SON but the effect is slightly stronger  
410 for SON, which also corresponds to reduced humidity for these areas (Fig. 8e-f; Fig. 9e-f).

411 The changes in precipitation show a distinct spatial and temporal pattern with changes in  
412 the rainbelt area (defined as 2mm day<sup>-1</sup> contour with 10-days smoothing, Fig. 11). Under  
413 future conditions, the rainbelt, which follows the ITCZ excursion, shifts around 3° northward  
414 during JAS (Fig. 11a). As a result, rainfall intensity increases from May to October, with the  
415 most pronounced increase by more than 30% relative to present-day levels of around 2 mm

416 day<sup>-1</sup> on the margins of the rainbelt. The rainy season becomes longer for Sahel (+9 days) as  
417 well as for central Africa (+1 day). The location of the rainbelt for the rest of the year  
418 remains unchanged, but there is a pronounced increase in rainfall intensity for the southern  
419 African rainy season (about 10%) and a decrease (about -10%) for the central African rainy  
420 seasons.

421 On top of the non-feedback climate change effect, vegetation feedbacks tend to cause a  
422 slight contraction of the rainbelt around the equator, and they impose a primarily  
423 counteractive effect on rainfall intensity compared to the climate change alone simulation  
424 (NFB). For central Africa, the considerable decrease in rainfall intensity in the dry season  
425 leads to a slight equatorward shrinking of the rainbelt (approximately 2°) and a shorter rainy  
426 season (on average 10 days, represented as a 4-day postponed onset and a 6-day earlier  
427 end). For southern Africa, strengthened convective precipitation results in a longer rainy  
428 season by on average 6 days. There is no pronounced effect for the Sahel regions except for  
429 some sparse changes over time and in some areas. To investigate the effects on ITCZ  
430 location, we analysed the position of the intertropical front (ITF) with a meridional wind  
431 criterion (Sultan and Janicot, 2003) by examining the location of maximum vertical uplifting  
432 wind speed at 850 hPa over Sahel in July and over southern Africa in January. However, we  
433 did not find pronounced effects for ITF (not shown) suggesting that changes in the rainbelt  
434 location for central Africa are mainly caused by changes in precipitation intensity rather  
435 than by changes in meridional circulation.

## 436 **4. Discussion**

### 437 **4.1 Related tenets of Regional Earth System Modelling**

438 We investigated the coupled dynamics of climate and vegetation over Africa under a future  
439 climate change scenario, applying a regional-scale ESM that dynamically couples a dynamic  
440 representation of vegetation structure, composition and distribution to a physical climate  
441 model at a comparatively high grid resolution. Uniquely among existing studies of climate  
442 dynamics for Africa, this enabled us to isolate the regional biophysical feedbacks, which are  
443 usually not easy to disentangle in a global application in which the effects of changes in  
444 carbon-cycle and large-scale circulation tend to compound the biophysical effects.

445 In comparison with global ESMs, the added value from the regional ESMs lies in the  
446 enhanced resolution obtained in a regional setup as presented in this study, allowing for a  
447 more detailed representation of local surface features such as topography, land use,  
448 vegetation change, and consequently possible related feedbacks, and also enhancing the  
449 model's ability to capture climatic variability and extreme climatic events (Giorgi,  
450 1995;Rummukainen, 2010, 2016). Improvements in the representation of local processes  
451 may be expected to result in improved larger scale features (e.g. sea level pressure,  
452 circulation patterns) (Diffenbaugh et al., 2005;Feser, 2006). For example, Kjellström et al.  
453 (2005) found that reduced bias in surface air temperature – largely determined by local  
454 energy balance – resulted in a better representation of interannual variability of mean sea  
455 level pressure and circulation patterns, and improved the simulation of precipitation.

## 456 **4.2 African vegetation patterns and change**

457 Vegetation dynamics are critically important in modulating the evolution of the 21st century  
458 climate in our study. Land use and grazing (Sankaran et al., 2005;Bondeau et al.,  
459 2007;Lindeskog et al., 2013), which were not included in our study, represent additional  
460 potentially important drivers of land surface changes. The historical vegetation state is also

461 relevant for future simulations, due to legacy effects lasting decades or even centuries  
462 (Moncrieff et al., 2014) and their influences on climate-vegetation equilibria (Claussen,  
463 1998;Wang and Eltahir, 2000). While our model exhibited a degree of bias in simulated  
464 vegetation under the present climate, the overall distribution of the major vegetation types  
465 of the continent (forest, savannah and grassland) was broadly correct. Arguably, vegetation  
466 type is a more important determinant of climate-vegetation equilibrium than structural  
467 parameters of a given type, such as LAI (Claussen, 1994;Wang and Eltahir, 2000).

468 Previous experimental (Kgope et al., 2010) and modelling (Sitch et al., 2008;Moncrieff et al.,  
469 2014) studies highlight the potential importance of physiological effects of atmospheric CO<sub>2</sub>  
470 concentrations on the productivity and water use efficiency of vegetation, particularly in low  
471 latitude and water-limited ecosystem types. Shrub encroachment and woody thickening has  
472 been observed in water-limited areas including Sahel in recent decades, coinciding with  
473 rising CO<sub>2</sub> concentrations (e.g. Liu et al., 2015). In our results, the simulated vegetation  
474 dynamics are consistent with these trends, presenting a trajectory of increased woody plant  
475 dominance (not shown), and a similar future vegetation pattern (Fig. 4) as in previous  
476 modelling studies (e.g., Sitch et al., 2008;Moncrieff et al., 2014). The vegetation changes  
477 simulated by our model under future climate forcing, are large relative to the bias noted in  
478 the representation of present-day vegetation state. This provides some confidence that the  
479 simulated future vegetation is not critically dependent on these biases and, in turn, that the  
480 emergent mechanisms of vegetation-climate interaction and their consequences for  
481 circulation and precipitation trends suggested by our study are robust.

### 482 ***4.3 Vegetation feedbacks and land-ocean temperature contrasts***

483 The land-ocean contrast is an important driver of continental precipitation, as it determines  
484 the transport of moisture from ocean to land (e.g. Giannini et al., 2003;Giannini et al.,  
485 2005;Fasullo, 2010;Boer, 2011;Lambert et al., 2011). The positive trend in Sahel rainfall over  
486 recent decades is a good example of linking moisture transport to land-ocean contrast,  
487 where changes in SSTs over adjacent tropical oceans around Africa are key to the fragile  
488 balance that defines the regional circulation system (Camberlin et al., 2001;Rowell,  
489 2001;Giannini et al., 2003). Land-surface feedback is found to modify the interannual to  
490 interdecadal climate variability in this region by vegetation-induced albedo or  
491 evapotranspiration effects (Zeng et al., 1999;Wang et al., 2004). In our study, the SSTs were  
492 prescribed from GCM-generated data, therefore the altered land-ocean thermal contrast  
493 between simulations with and without feedback originated solely from the changes in land  
494 surface temperature, in turn attributable to vegetation dynamics. Although this represents a  
495 land-forced mechanism in contrast to an ocean-forced one inferred in other studies (e.g.  
496 Giannini et al., 2003;Tokinaga et al., 2012), the mechanisms are similar. Wind speed and  
497 land-ocean temperature contrast are reduced by approximately by  $0.2 \text{ m s}^{-1}$  and  $0.2^\circ\text{C}$ ,  
498 respectively, when vegetation feedbacks are enabled in our study (Fig. 5 and Table A2);  
499 these are comparable to the changes simulated in other studies for the Sahel  
500 (approximately  $0.2\text{-}0.5 \text{ m s}^{-1}$  per  $0.2^\circ\text{C}$  (Giannini et al., 2005)) and for the Pacific Oceans  
501 (approximately  $0.3 \text{ m s}^{-1}$  per  $0.3^\circ\text{C}$  (Tokinaga et al., 2012)). However, the relative importance  
502 of such changes may differ for local climate systems: the lower branch of the Walker cell  
503 over the eastern tropical Atlantic Ocean, which we have focused on in this study, may be in  
504 a fragile balance and is more vulnerable to changes in thermal contrasts (equatorial  
505 westerlies slowed down by approximately  $0.2 \text{ m s}^{-1}$  from less than  $2 \text{ m s}^{-1}$  of the present-day  
506 wind speed in rainy seasons, Table A2) compared to the stronger monsoonal circulation for

507 Sahel and the Walker cell over the equatorial Pacific Ocean (> 5 m per second wind speed in  
508 their peak months, Young, 1999). Our results indicate that even a small disturbance of the  
509 eastern Tropical Atlantic circulation cell may produce profound impacts (larger relative  
510 reduction in precipitation compared with the studies by Giannini et al. (2005) and Tokinaga  
511 et al. (2012)).

512 Despite biases in the initial precipitation and vegetation state (LAI) for some regions, our  
513 model was able to reproduce the present-day land cover type, and the simulated present-  
514 date climate is close to previous study (Nikulin et al., 2012) using the same physical sub-  
515 model with observed land cover type. Under future climate change, vegetation-induced  
516 changes in circulation, thus a substantial change in moisture transport and precipitation, are  
517 mainly triggered by changes in land cover type (Fig. 4a), therefore, we argue that the  
518 influences from biases in initial conditions on such mechanism found in this study should be  
519 limited. Our study used prescribed SST forcing from a GCM and could thus not account for  
520 additional or opposing feedbacks mediated by ocean dynamics. However, as the ocean heat  
521 capacity is relatively large and variation in land-ocean thermal contrast can be greatly  
522 buffered by ocean heat uptake (Lambert and Chiang, 2007), we suggest that results should  
523 not change fundamentally if a dynamic ocean component was introduced to the model.

## 524 ***5. Conclusion and outlook***

525 We investigated the potential role of vegetation-mediated biophysical feedbacks on climate  
526 change projections for Africa in the 21<sup>st</sup> century. In current savannah regions, enhanced  
527 forest growth results in a strong evaporative cooling effect. We also identify alterations in  
528 the large-scale circulation induced by savannah vegetation change, resulting in remote

529 effects and modulation of tropical rainfall patterns over Africa, favouring savannah  
530 ecosystems at the expense of equatorial rainforest. Our results point to the potential  
531 importance of vegetation-atmosphere interactions for regional climate dynamics and trends,  
532 and motivate the incorporation of vegetation dynamics and land-atmosphere biophysical  
533 coupling in regional models. This has become the standard in global climate modelling, but  
534 remains rare in regional climate modelling.

535 Future work can include detailed studies on the role of vegetation feedbacks in the regional  
536 climate projections with respect to shorter-term dynamics such as climate variability and  
537 extreme events, which may have crucial implications for landscape processes such as  
538 wildfire. Regional and global biogeochemical feedbacks on future climate change may be  
539 triggered by regional biophysical feedbacks, with implications for regional climatic trends,  
540 variability and seasonality under future greenhouse forcing (Zhang et al., 2014). Impacts on  
541 the carbon balance of semi-arid ecosystem like savannahs, known to respond sensitively to  
542 variations in rainfall (Ahlström et al., 2015) may be particularly relevant to address for Africa.  
543 The development of regional ESMs to account for the impacts of land use interventions such  
544 as afforestation and reforestation, as well as forest clearing, grazing and fire management  
545 may be a valuable next step, enabling land surface-atmosphere interaction studies linked to  
546 socioeconomic scenarios and climate change mitigation strategies.

547

548

549

550



551 ***Appendix A: Description of the coupling between RCA and LPJ-GUESS***

552 In RCA-GUESS, the LSS in RCA is coupled with LPJ-GUESS, which feeds back vegetation  
553 properties to RCA. RCA provides net downward shortwave radiation, air temperature,  
554 precipitation to LPJ-GUESS. In return, LPJ-GUESS provides daily updated LAI and the annually  
555 updated tile sizes (determined from the simulated maximum growing season LAI summed  
556 across tree and herbaceous PFTs in the previous year (Smith et al., 2011)). In the forest tile  
557 in RCA, vegetation cover in this tile is estimated as the foliar projective cover (FPC) using  
558 Beer's law:

559 
$$A_{tree} = 1.0 - \exp(-0.5 \cdot LAI_{tree}), \quad (1)$$

560 where  $LAI_{tree}$  is the aggregated LAI of woody species, simulated by LPJ-GUESS in its forest  
561 tile in which vegetation is assumed to comprise trees and understory herbaceous vegetation.

562 The natural vegetated fraction of the open land tile was calculated similarly:

564 
$$A_{grass} = 1.0 - \exp(-0.5 \cdot LAI_{grass}), \quad (2)$$

565 where  $LAI_{grass}$  is the summed LAI of the simulated herbaceous PFTs from the herbaceous  
566 tile of LPJ-GUESS in which only herbaceous vegetation is allowed to grow. The relative  
567 covers of the forest and open land tiles affect surface albedo, which is a weighted average  
568 of prescribed albedo constants for forest, open land and bare soil and controls the  
569 absorption of surface incoming solar radiation, and therefore influences surface energy  
570 balance and temperature.

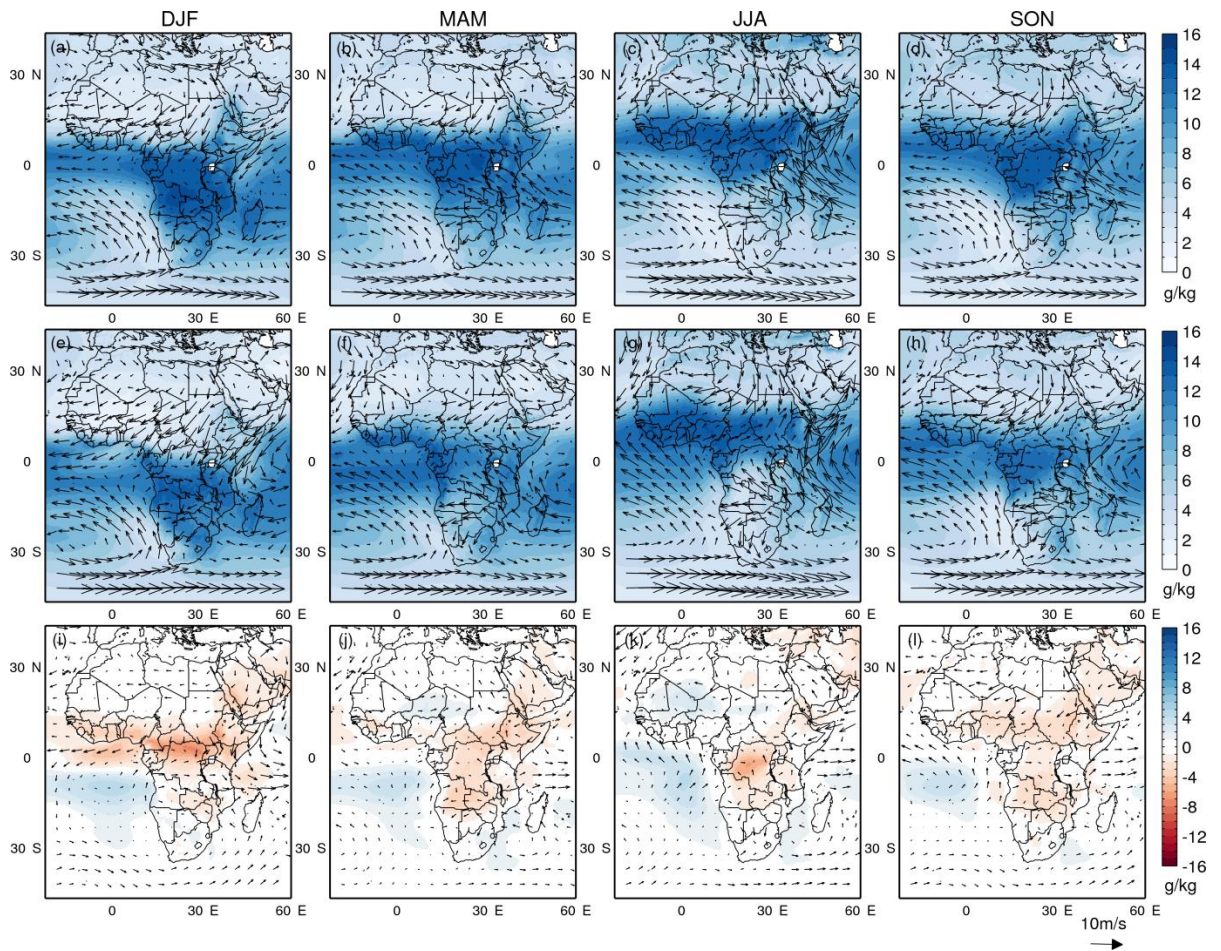
572 The turbulent heat fluxes are influenced by the properties of each tile, such as surface  
573 roughness and surface resistance, which partly depend on vegetation properties provided  
574 by LPJ-GUESS. The vegetation surface resistance controls vegetation transpiration and bare  
575 soil evaporation for latent heat flux calculation. It scales with LAI and varies between the

576 different types of vegetation and affected by the incoming photosynthetically active  
577 radiation, soil-water stress, vapour pressure deficit, air temperature and soil temperature.  
578 The aerodynamic resistance controls both latent heat flux and sensible heat flux and is  
579 influenced by surface roughness length distinguished from open land and forest. The total  
580 heat fluxes and heat transfer determine the time evolution of the surface temperature and  
581 thus the thermodynamics in the lower boundary layer. More details about the LSS are given  
582 in Samuelsson et al. (2006), and the description of its coupling to the vegetation sub-model  
583 is provided by Smith et al. (2011).

584 Table A1. Characteristics of the plant functional types (PFTs) used in the vegetation sub-model LPJ-GUESS.

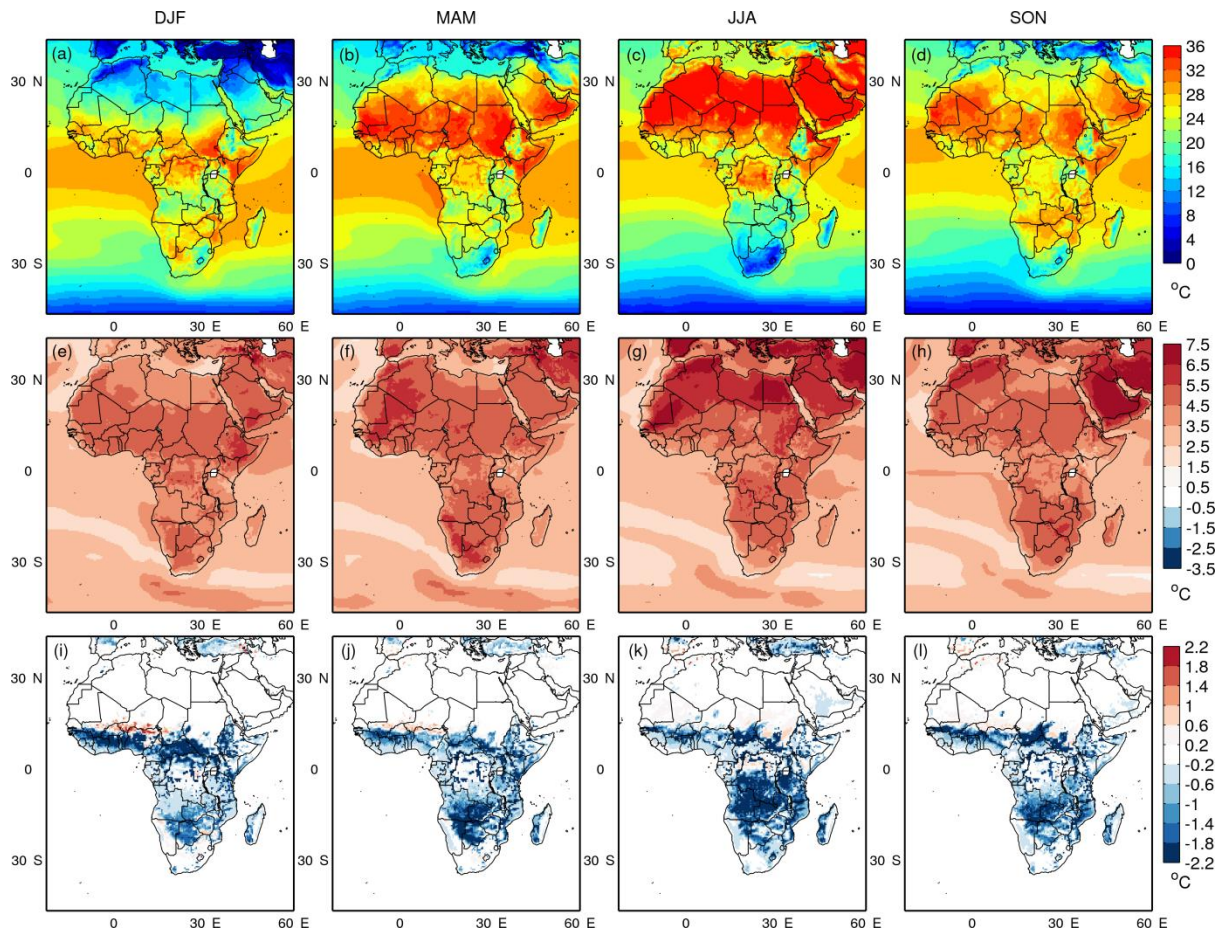
Characteristics	NE	BE	TrBE	TrBR	TBS	IBS	C3G	C4G
Leaf phenology <sup>a</sup>	E	E	E	D	D	D	R	R
Drought tolerance	low	low	low	low	low	low	very low	very low
Shade tolerance	high	high	high	low	high	low	low	Low
Optimal temperature range for photosynthesis (°C)	10-25	15-35	25-30	25-30	15-25	10-25	10-30	20-45
Min T <sub>c</sub> for survival (°C) <sup>b</sup>	-	1.7	15.5	15.5	-18	-	-	15.5

585 Notes: NE, needleleaved evergreen tree; BE, broadleaved evergreen tree; TrBE, tropical broadleaved  
586 evergreen tree; TrBR, tropical broadleaved raingreen tree; TBS, shade-tolerant broadleaved summergreen tree;  
587 IBS, shade-intolerant broadleaved summergreen tree; C3G, C3 grass or herb; C4G, C4 grass or herb;  
588 <sup>a</sup>E, evergreen; D, deciduous; R, raingreen.  
589 <sup>b</sup>T<sub>c</sub> = mean temperature (°C) of coldest month of year.



590

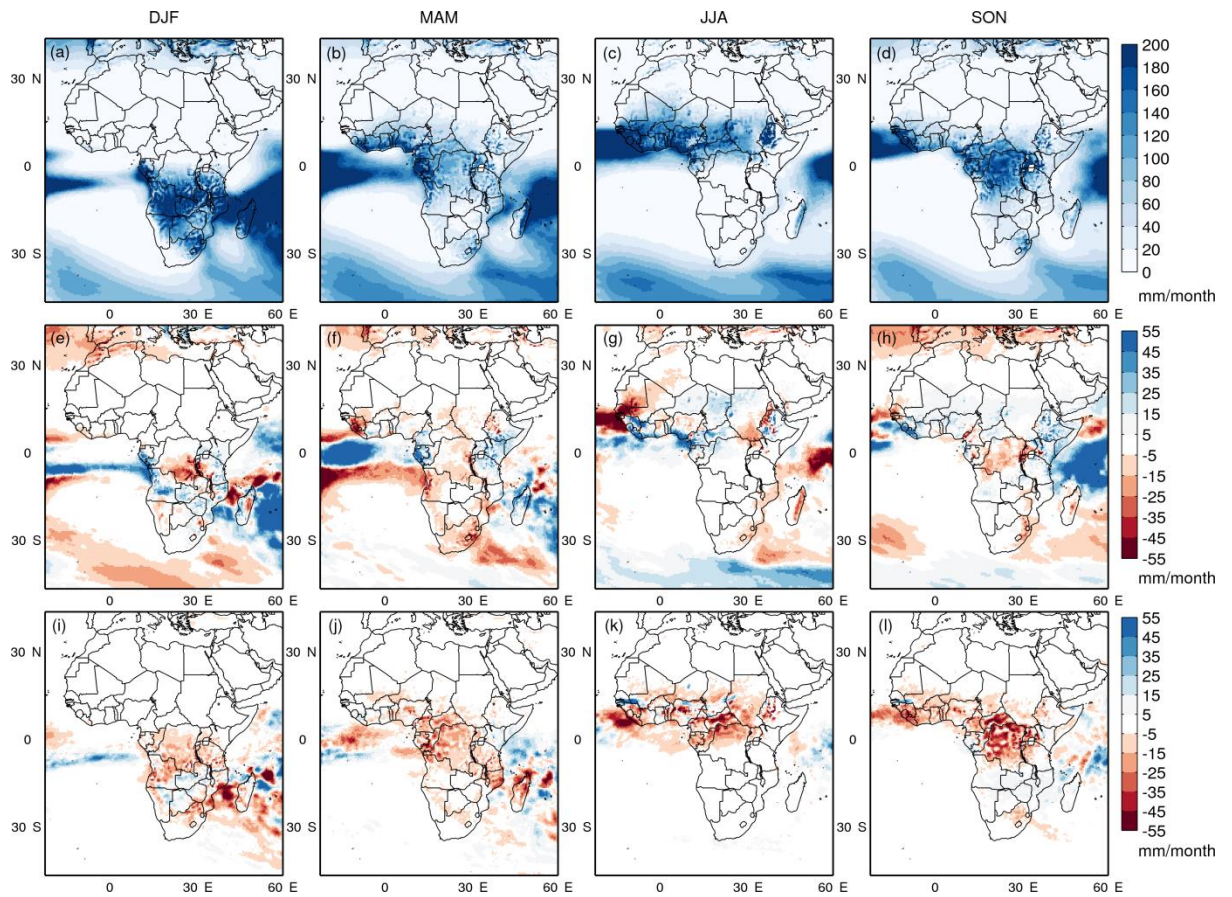
591 Fig. A1. Seasonal atmospheric circulation (arrows,  $\text{m s}^{-1}$ ) and specific humidity (colour contours,  $\text{g kg}^{-1}$ ) at  
 592 850 hPa pressure level from ERA-Interim (1<sup>st</sup> row), NFB run (2<sup>nd</sup> row), as well as their differences (3<sup>rd</sup> row, NFB  
 593 minus ERA-Interim), for the period 1997-2010.



594

595 Fig. A2. Simulated seasonal surface temperature for present day (a-d), for changes in future in the NFB  
 596 experiment (e-h, future minus present day), and for changes from vegetation feedback in future (i-l, FB minus  
 597 NFB for future). Definitions for calculation period, climate change signal and vegetation feedbacks are given in  
 598 Sect. 2.2.

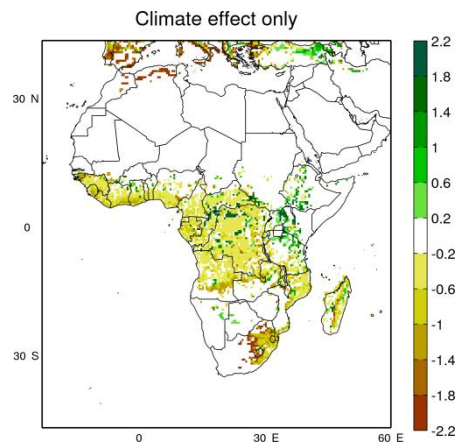
599



600

601

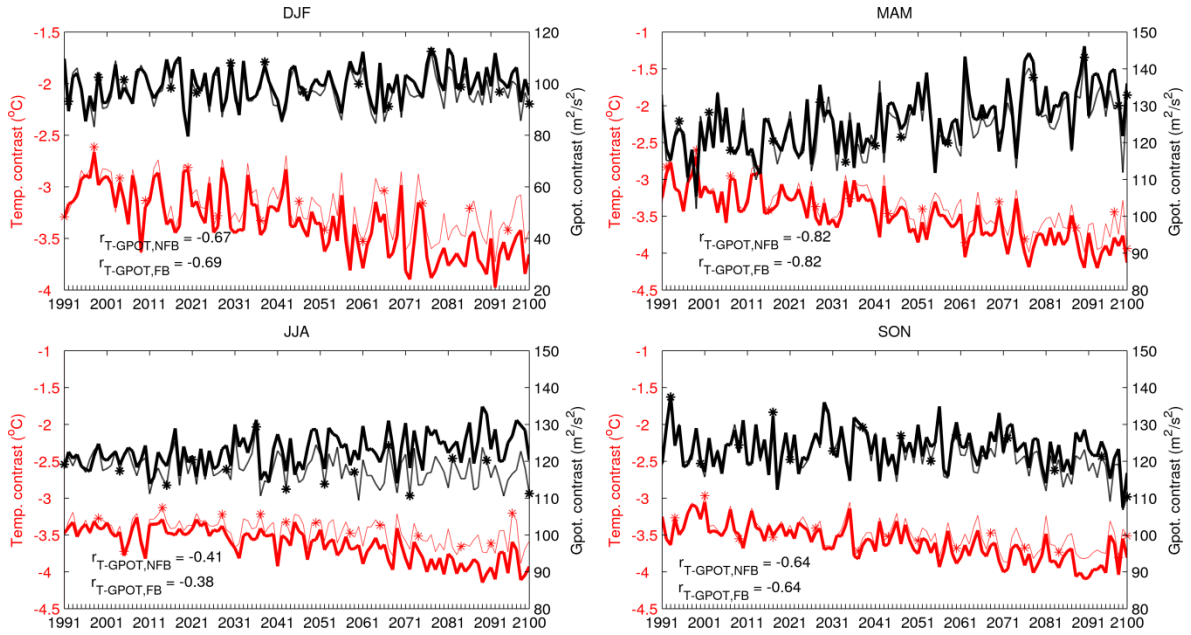
Fig. A3. Similar to Fig. A2., but for precipitation.



602

603

Fig. A4. Changes in forest tile LAI from the period 1991-2010 to the period 2081-2100 in FB\_CC experiment.



604

605 Fig. A5. Annual changes in atmospheric ocean-land temperature contrast ( $\nabla T$ ) and geopotential contrast  
 606 ( $\nabla \phi$ ) in time series for four seasons, represented by the mean contrast at the three pressure levels 850, 925  
 607 and 975 hPa (ocean minus land) within the domain 15°N-15°S, 24°W-20°E (see the inset in the panel for JJA in  
 608 Fig. 5). Correlation coefficient ( $r$ ) between atmospheric temperature contrast ( $\nabla T$ ) and geopotential contrast  
 609 ( $\nabla \phi$ ) are computed based on the de-trended annual time-series values for both FB (thick lines) and NFB (thin  
 610 lines with asterisks) simulations. Changes between FB and NFB are significant at 95% confidence level for the  
 611 whole time period. Note the different y-axis for DJF.

612 Table A2. Atmospheric temperature contrast, geopotential contrast and westerlies wind speed for the  
 613 present-day state and contributions from climate change (CC subscript) and vegetation feedbacks (FB  
 614 subscript), standard deviation is in parenthesis.

	DJF	MAM	JJA	SON
$\nabla T_{\text{present-day}} (^{\circ}\text{C})^a$	-3.06 (0.30)	-3.15 (0.34)	-3.47 (0.22)	-3.37 (0.24)
$\Delta \nabla T_{\text{CC}} (^{\circ}\text{C})^a$	-0.59*	-0.73*	-0.45*	-0.47*
$\Delta \nabla T_{\text{FB}} (^{\circ}\text{C})^a$	0.29*	0.23*	0.31*	0.22*
$\nabla \phi_{\text{present-day}} (\text{m}^2 \text{s}^{-2})^a$	98.14 (5.92)	120.86 (7.03)	120.94 (3.83)	124.08 (4.58)
$\Delta \nabla \phi_{\text{CC}} (\text{m}^2 \text{s}^{-2})^a$	3.94	11.96*	4.73*	-3.32
$\Delta \nabla \phi_{\text{FB}} (\text{m}^2 \text{s}^{-2})^a$	-4.93*	-3.86*	-8.96*	-3.92*
$U_{\text{zonal,present-day}} (\text{m s}^{-1})^b$	0.01 (0.27)	1.47 (0.32)	0.87 (0.37)	1.22 (0.31)
$\Delta U_{\text{zonal,CC}} (\text{m s}^{-1})^b$	0.35*	0.32*	0.68*	0.17*
$\Delta U_{\text{zonal,FB}} (\text{m s}^{-1})^b$	-0.00	-0.21*	-0.28*	-0.16*

615 Note: <sup>a</sup>: Calculations are same as Fig. 5.

616 <sup>b</sup>:  $U_{\text{zonal}}$  is the averaged zonal wind speed for the pressure levels 850, 925 and 975 hPa between 3.5°N-6.5°N and 0-10°E;  
 617 The positive represents westerly and the negative represents easterly.

618 \*: Changes are significant at 95% confidence level using Mann-Whitney U-test (Hollander and Wolfe, 1999).

619

620

621 ***Acknowledgement***

622 This study is a contribution to the strategic research areas Modelling the Regional and  
623 Global Earth System (MERGE) and Biodiversity and Ecosystem Services in a Changing Climate  
624 (BECC). MCW would like to thank Paul Miller and Grigory Nikulin for their helpful discussions  
625 and comments on this work. The model simulations were performed at the National  
626 Supercomputer Centre (NSC) in Linköping, Sweden.

627

628

629

630

631

632

633

634

635

636

637

638

639 **Reference**

- 640 Ahlström, A., Raupach, M. R., Schurgers, G., Smith, B., Arneeth, A., Jung, M.,  
641 Reichstein, M., Canadell, J. G., Friedlingstein, P., and Jain, A. K.: The  
642 dominant role of semi-arid ecosystems in the trend and variability of the  
643 land CO<sub>2</sub> sink, *Science*, 348, 895-899, 2015.
- 644 Alo, C. A., and Wang, G.: Role of dynamic vegetation in regional climate  
645 predictions over western Africa, *Climate dynamics*, 35, 907-922, 2010.
- 646 Anav, A., Friedlingstein, P., Kidston, M., Bopp, L., Ciais, P., Cox, P., Jones, C.,  
647 Jung, M., Myneni, R., and Zhu, Z.: Evaluating the Land and Ocean  
648 Components of the Global Carbon Cycle in the CMIP5 Earth System Models,  
649 *Journal of Climate*, 26, 6801-6843, 10.1175/jcli-d-12-00417.1, 2013.
- 650 Arora, V., Scinocca, J., Boer, G., Christian, J., Denman, K., Flato, G., Kharin, V.,  
651 Lee, W., and Merryfield, W.: Carbon emission limits required to satisfy  
652 future representative concentration pathways of greenhouse gases,  
653 *Geophysical Research Letters*, 38, 2011.
- 654 Avissar, R., and Werth, D.: Global hydroclimatological teleconnections  
655 resulting from tropical deforestation, *Journal of Hydrometeorology*, 6, 134-  
656 145, 2005.
- 657 Berrisford, P., Dee, D., Fielding, K., Fuentes, M., Kallberg, P., Kobayashi, S.,  
658 and Uppala, S.: The ERA-Interim Archive, 2009.
- 659 Boer, G.: The ratio of land to ocean temperature change under global  
660 warming, *Climate dynamics*, 37, 2253-2270, 2011.
- 661 Bonan, G. B.: Forests and climate change: forcings, feedbacks, and the  
662 climate benefits of forests, *science*, 320, 1444-1449, 2008.
- 663 Bondeau, A., Smith, P. C., Zaehle, S., Schaphoff, S., Lucht, W., Cramer, W.,  
664 Gerten, D., LOTZE - CAMPEN, H., Müller, C., and Reichstein, M.: Modelling  
665 the role of agriculture for the 20th century global terrestrial carbon balance,  
666 *Global Change Biology*, 13, 679-706, 2007.
- 667 Brovkin, V., Claussen, M., Driesschaert, E., Fichefet, T., Kicklighter, D., Loutre,  
668 M.-F., Matthews, H., Ramankutty, N., Schaeffer, M., and Sokolov, A.:  
669 Biogeophysical effects of historical land cover changes simulated by six  
670 Earth system models of intermediate complexity, *Climate Dynamics*, 26,  
671 587-600, 2006.
- 672 Camberlin, P., Janicot, S., and Pocard, I.: Seasonality and atmospheric  
673 dynamics of the teleconnection between African rainfall and tropical sea -  
674 surface temperature: Atlantic vs. ENSO, *International Journal of*  
675 *Climatology*, 21, 973-1005, 2001.
- 676 Charney, J. G.: Dynamics of deserts and drought in the Sahel, *Quarterly*  
677 *Journal of the Royal Meteorological Society*, 101, 193-202, 1975.



678 Claussen, M.: On coupling global biome models with climate models,  
679 *Climate Research*, 4, 203-221, 1994.

680 Claussen, M.: Modeling bio-geophysical feedback in the African and Indian  
681 monsoon region, *Climate Dynamics*, 13, 247-257, 1997.

682 Claussen, M.: On multiple solutions of the atmosphere – vegetation system  
683 in present - day climate, *Global Change Biology*, 4, 549-559, 1998.

684 Claussen, M., and Gayler, V.: The greening of the Sahara during the mid-  
685 Holocene: results of an interactive atmosphere-biome model, *Global*  
686 *Ecology and Biogeography Letters*, 369-377, 1997.

687 Cook, K. H., and Vizy, E. K.: The Congo Basin Walker circulation: dynamics  
688 and connections to precipitation, *Climate Dynamics*, 1-21, 2015.

689 Dezfuli, A. K., and Nicholson, S. E.: The relationship of rainfall variability in  
690 western equatorial Africa to the tropical oceans and atmospheric  
691 circulation. Part II: The boreal autumn, *Journal of Climate*, 26, 66-84, 2013.

692 Diffenbaugh, N. S., Pal, J. S., Trapp, R. J., and Giorgi, F.: Fine-scale processes  
693 regulate the response of extreme events to global climate change,  
694 *Proceedings of the National Academy of Sciences of the United States of*  
695 *America*, 102, 15774-15778, 10.1073/pnas.0506042102, 2005.

696 Döscher, R., Wyser, K., Meier, H. M., Qian, M., and Redler, R.: Quantifying  
697 Arctic contributions to climate predictability in a regional coupled ocean-  
698 ice-atmosphere model, *Climate Dynamics*, 34, 1157-1176, 2010.

699 Eklundh, L., and Olsson, L.: Vegetation index trends for the African Sahel  
700 1982–1999, *Geophysical Research Letters*, 30, 2003.

701 Eltahir, E. A.: Role of vegetation in sustaining large-scale atmospheric  
702 circulations in the tropics, *JOURNAL OF GEOPHYSICAL RESEARCH-ALL*  
703 *SERIES-*, 101, 4255-4268, 1996.

704 Fasullo, J. T.: Robust Land-Ocean Contrasts in Energy and Water Cycle  
705 Feedbacks\*, *Journal of Climate*, 23, 4677-4693, 2010.

706 Feser, F.: Enhanced detectability of added value in limited-area model  
707 results separated into different spatial scales, *Monthly weather review*, 134,  
708 2180-2190, 2006.

709 Giannini, A., Saravanan, R., and Chang, P.: Oceanic forcing of Sahel rainfall  
710 on interannual to interdecadal time scales, *Science*, 302, 1027-1030, 2003.

711 Giannini, A., Saravanan, R., and Chang, P.: Dynamics of the boreal summer  
712 African monsoon in the NSIPP1 atmospheric model, *Climate Dynamics*, 25,  
713 517-535, 2005.

714 Giorgi, F.: Perspectives for regional earth system modeling, *Global and*  
715 *Planetary Change*, 10, 23-42, 1995.

716 Giorgi, F., Jones, C., and Asrar, G. R.: Addressing climate information needs  
717 at the regional level: the CORDEX framework, *World Meteorological*  
718 *Organization (WMO) Bulletin*, 58, 175, 2009.

719 Harris, I., Jones, P. D., Osborn, T. J., and Lister, D. H.: Updated high-  
720 resolution grids of monthly climatic observations – the CRU TS3.10 Dataset,  
721 *International Journal of Climatology*, 34, 623-642, 10.1002/joc.3711, 2014.

722 Herrmann, S. M., Anyamba, A., and Tucker, C. J.: Recent trends in vegetation  
723 dynamics in the African Sahel and their relationship to climate, *Global*  
724 *Environmental Change*, 15, 394-404,  
725 <http://dx.doi.org/10.1016/j.gloenvcha.2005.08.004>, 2005.

726 Hickler, T., Eklundh, L., Seaquist, J. W., Smith, B., Ardö, J., Olsson, L., Sykes, M.  
727 T., and Sjöström, M.: Precipitation controls Sahel greening trend,  
728 *Geophysical Research Letters*, 32, 2005.

729 Hickler, T., Smith, B., Prentice, I. C., Mjofors, K., Miller, P., Arneth, A., and  
730 Sykes, M. T.: CO<sub>2</sub> fertilization in temperate FACE experiments not  
731 representative of boreal and tropical forests, *Global Change Biology*, 14,  
732 1531-1542, 10.1111/j.1365-2486.2008.01598.x, 2008.

733 Hickler, T., Vohland, K., Feehan, J., Miller, P. A., Smith, B., Costa, L., Giesecke,  
734 T., Fronzek, S., Carter, T. R., and Cramer, W.: Projecting the future  
735 distribution of European potential natural vegetation zones with a  
736 generalized, tree species - based dynamic vegetation model, *Global Ecology*  
737 *and Biogeography*, 21, 50-63, 2012.

738 Hollander, M., and Wolfe, D. A.: in: *Nonparametric Statistical Methods*, 2nd  
739 ed., John Wiley & Sons, New York 35-140, 1999.

740 Huffman, G. J., Adler, R. F., Morrissey, M. M., Bolvin, D. T., Curtis, S., Joyce, R.,  
741 McGavock, B., and Susskind, J.: Global precipitation at one-degree daily  
742 resolution from multisatellite observations, *Journal of Hydrometeorology*,  
743 2, 36-50, 2001.

744 Jamali, S., Seaquist, J., Eklundh, L., and Ardö, J.: Automated mapping of  
745 vegetation trends with polynomials using NDVI imagery over the Sahel,  
746 *Remote Sensing of Environment*, 141, 79-89,  
747 <http://dx.doi.org/10.1016/j.rse.2013.10.019>, 2014.

748 Jones, C., Giorgi, F., and Asrar, G.: The Coordinated Regional Downscaling  
749 Experiment: CORDEX—an international downscaling link to CMIP5, *Clivar*  
750 *Exchanges*, 16, 34-40, 2011.

751 Joshi, M. M., Gregory, J. M., Webb, M. J., Sexton, D. M., and Johns, T. C.:  
752 Mechanisms for the land/sea warming contrast exhibited by simulations of  
753 climate change, *Climate Dynamics*, 30, 455-465, 2008.

754 Keenan, T. F., Hollinger, D. Y., Bohrer, G., Dragoni, D., Munger, J. W., Schmid,  
755 H. P., and Richardson, A. D.: Increase in forest water-use efficiency as  
756 atmospheric carbon dioxide concentrations rise, *Nature*, 499, 324-327,  
757 2013.

758 Kgope, B. S., Bond, W. J., and Midgley, G. F.: Growth responses of African  
759 savanna trees implicate atmospheric [CO<sub>2</sub>] as a driver of past and current  
760 changes in savanna tree cover, *Austral Ecology*, 35, 451-463, 2010.

761 Kjellström, E., Bärring, L., Gollvik, S., Hansson, U., Jones, C., Samuelsson, P.,  
762 Rummukainen, M., Ullerstig, A., Willén, U., and Wyser, K.: A 140-year  
763 simulation of European climate with the new version of the Rossby Centre  
764 regional atmospheric climate model (RCA3), 2005.

765 Kjellström, E., Nikulin, G., Hansson, U., Strandberg, G., and Ullerstig, A.: 21st  
766 century changes in the European climate: uncertainties derived from an  
767 ensemble of regional climate model simulations, *Tellus A*, 63, 24-40, 2011.

768 Kucharski, F., Zeng, N., and Kalnay, E.: A further assessment of vegetation  
769 feedback on decadal Sahel rainfall variability, *Climate dynamics*, 40, 1453-  
770 1466, 2013.

771 Lambert, F. H., and Chiang, J. C.: Control of land - ocean temperature  
772 contrast by ocean heat uptake, *Geophysical research letters*, 34, 2007.

773 Lambert, F. H., Webb, M. J., and Joshi, M. M.: The relationship between land-  
774 ocean surface temperature contrast and radiative forcing, *Journal of*  
775 *Climate*, 24, 3239-3256, 2011.

776 LaRow, T. E., Stefanova, L., and Seitz, C.: Dynamical simulations of north  
777 Atlantic tropical cyclone activity using observed low-frequency SST  
778 oscillation imposed on CMIP5 Model RCP4. 5 SST projections, *Journal of*  
779 *Climate*, 27, 8055-8069, 2014.

780 Lawrence, D., and Vandecar, K.: Effects of tropical deforestation on climate  
781 and agriculture, *Nature Climate Change*, 5, 27-36, 2015.

782 Lindeskog, M., Arneeth, A., Bondeau, A., Waha, K., Seaquist, J., Olin, S., and  
783 Smith, B.: Implications of accounting for land use in simulations of  
784 ecosystem carbon cycling in Africa, *Earth System Dynamics*, 4, 385-407,  
785 2013.

786 Liu, Y. Y., van Dijk, A. I. J. M., de Jeu, R. A. M., Canadell, J. G., McCabe, M. F.,  
787 Evans, J. P., and Wang, G.: Recent reversal in loss of global terrestrial  
788 biomass, *Nature Clim. Change*, 5, 470-474, 10.1038/nclimate2581  
789 [http://www.nature.com/nclimate/journal/v5/n5/abs/nclimate2581.html](http://www.nature.com/nclimate/journal/v5/n5/abs/nclimate2581.html#supplementary-information)  
790 [#supplementary-information](http://www.nature.com/nclimate/journal/v5/n5/abs/nclimate2581.html#supplementary-information), 2015.

791 Long, S.: Modification of the response of photosynthetic productivity to  
792 rising temperature by atmospheric CO<sub>2</sub> concentrations: has its importance  
793 been underestimated?, *Plant, Cell & Environment*, 14, 729-739, 1991.

794 Moncrieff, G. R., Scheiter, S., Bond, W. J., and Higgins, S. I.: Increasing  
795 atmospheric CO<sub>2</sub> overrides the historical legacy of multiple stable biome  
796 states in Africa, *New Phytologist*, 201, 908-915, 2014.

797 Morales, P., Hickler, T., Rowell, D. P., Smith, B., and Sykes, M. T.: Changes in  
798 European ecosystem productivity and carbon balance driven by regional  
799 climate model output, *Global Change Biology*, 13, 108-122, 2007.

800 Moss, R. H., Edmonds, J. A., Hibbard, K. A., Manning, M. R., Rose, S. K., Van  
801 Vuuren, D. P., Carter, T. R., Emori, S., Kainuma, M., and Kram, T.: The next

802 generation of scenarios for climate change research and assessment,  
803 Nature, 463, 747-756, 2010.

804 Nicholson, S. E., and Grist, J. P.: The seasonal evolution of the atmospheric  
805 circulation over West Africa and equatorial Africa, Journal of Climate, 16,  
806 1013-1030, 2003.

807 Nikulin, G., Jones, C., Giorgi, F., Asrar, G., Büchner, M., Cerezo-Mota, R.,  
808 Christensen, O. B., Déqué, M., Fernandez, J., Hänsler, A., van Meijgaard, E.,  
809 Samuelsson, P., Sylla, M. B., and Sushama, L.: Precipitation Climatology in an  
810 Ensemble of CORDEX-Africa Regional Climate Simulations, Journal of  
811 Climate, 25, 6057-6078, 10.1175/JCLI-D-11-00375.1, 2012.

812 Nogherotto, R., Coppola, E., Giorgi, F., and Mariotti, L.: Impact of Congo  
813 Basin deforestation on the African monsoon, Atmospheric Science Letters,  
814 14, 45-51, 2013.

815 Olsson, L., Eklundh, L., and Ardö, J.: A recent greening of the Sahel—trends,  
816 patterns and potential causes, Journal of Arid Environments, 63, 556-566,  
817 2005.

818 Pokam, W. M., Bain, C. L., Chadwick, R. S., Graham, R., Sonwa, D. J., and  
819 Kamga, F. M.: Identification of processes driving low-level westerlies in  
820 West Equatorial Africa, Journal of Climate, 27, 4245-4262, 2014.

821 Rowell, D. P.: Teleconnections between the tropical Pacific and the Sahel,  
822 Quarterly Journal of the Royal Meteorological Society, 127, 1683-1706,  
823 2001.

824 Rowell, D. P.: Simulating SST teleconnections to Africa: What is the state of  
825 the art?, Journal of Climate, 26, 5397-5418, 2013.

826 Rummukainen, M.: State-of-the-art with regional climate models, Wiley  
827 Interdisciplinary Reviews: Climate Change, 1, 82-96, 10.1002/wcc.8, 2010.

828 Rummukainen, M.: Added value in regional climate modeling, Wiley  
829 Interdisciplinary Reviews: Climate Change, 7, 145-159, 10.1002/wcc.378,  
830 2016.

831 Samuelsson, P., Gollvik, S., and Ullerstig, A.: The land-surface scheme of the  
832 Rossby Centre regional atmospheric climate model (RCA3), SMHI, 2006.

833 Samuelsson, P., Jones, C. G., Willén, U., Ullerstig, A., Gollvik, S., Hansson, U.,  
834 Jansson, C., Kjellström, E., Nikulin, G., and Wyser, K.: The Rossby Centre  
835 Regional Climate model RCA3: model description and performance, Tellus  
836 A, 63, 4-23, 2011.

837 Sankaran, M., Hanan, N. P., Scholes, R. J., Ratnam, J., Augustine, D. J., Cade, B.  
838 S., Gignoux, J., Higgins, S. I., Le Roux, X., and Ludwig, F.: Determinants of  
839 woody cover in African savannas, Nature, 438, 846-849, 2005.

840 Schefuß, E., Schouten, S., and Schneider, R. R.: Climatic controls on central  
841 African hydrology during the past 20,000 years, Nature, 437, 1003-1006,  
842 2005.

843 Scheiter, S., and Higgins, S. I.: Impacts of climate change on the vegetation of  
844 Africa: an adaptive dynamic vegetation modelling approach, *Global Change*  
845 *Biology*, 15, 2224-2246, 2009.

846 Sitch, S., Huntingford, C., Gedney, N., Levy, P. E., Lomas, M., Piao, S. L., Betts,  
847 R., Ciais, P., Cox, P., Friedlingstein, P., Jones, C. D., Prentice, I. C., and  
848 Woodward, F. I.: Evaluation of the terrestrial carbon cycle, future plant  
849 geography and climate-carbon cycle feedbacks using five Dynamic Global  
850 Vegetation Models (DGVMs), *Global Change Biology*, 14, 2015-2039,  
851 10.1111/j.1365-2486.2008.01626.x, 2008.

852 Smith, B., Prentice, I. C., and Sykes, M. T.: Representation of vegetation  
853 dynamics in the modelling of terrestrial ecosystems: comparing two  
854 contrasting approaches within European climate space, *Global Ecology and*  
855 *Biogeography*, 10, 621-637, 10.1046/j.1466-822X.2001.t01-1-00256.x,  
856 2001.

857 Smith, B., Samuelsson, P., Wramneby, A., and Rummukainen, M.: A model of  
858 the coupled dynamics of climate, vegetation and terrestrial ecosystem  
859 biogeochemistry for regional applications, *Tellus A*, 63, 87-106,  
860 10.1111/j.1600-0870.2010.00477.x, 2011.

861 Smith, B., Warlind, D., Arneeth, A., Hickler, T., Leadley, P., Siltberg, J., and  
862 Zaehle, S.: Implications of incorporating N cycling and N limitations on  
863 primary production in an individual-based dynamic vegetation model,  
864 *Biogeosciences*, 11, 2027-2054, 2014.

865 Sörensson, A. A., and Menéndez, C. G.: Summer soil–precipitation coupling  
866 in South America, *Tellus A*, 63, 56-68, 2011.

867 Sultan, B., and Janicot, S.: The West African monsoon dynamics. Part II: The  
868 “preonset” and “onset” of the summer monsoon, *Journal of climate*, 16,  
869 3407-3427, 2003.

870 Sutton, R. T., Dong, B., and Gregory, J. M.: Land/sea warming ratio in  
871 response to climate change: IPCC AR4 model results and comparison with  
872 observations, *Geophysical Research Letters*, 34, n/a-n/a,  
873 10.1029/2006GL028164, 2007.

874 Sylla, M., Giorgi, F., Ruti, P., Calmanti, S., and Dell'Aquila, A.: The impact of  
875 deep convection on the West African summer monsoon climate: a regional  
876 climate model sensitivity study, *Quarterly Journal of the Royal*  
877 *Meteorological Society*, 137, 1417-1430, 2011.

878 Taylor, K. E., Stouffer, R. J., and Meehl, G. A.: An overview of CMIP5 and the  
879 experiment design, *Bulletin of the American Meteorological Society*, 93,  
880 485-498, 2012.

881 Texier, D., De Noblet, N., Harrison, S., Haxeltine, A., Jolly, D., Jousaume, S.,  
882 Laarif, F., Prentice, I., and Tarasov, P.: Quantifying the role of biosphere-  
883 atmosphere feedbacks in climate change: coupled model simulations for

884 6000 years BP and comparison with palaeodata for northern Eurasia and  
885 northern Africa, *Climate Dynamics*, 13, 865-881, 1997.

886 Thonicke, K., Venevsky, S., Sitch, S., and Cramer, W.: The role of fire  
887 disturbance for global vegetation dynamics: coupling fire into a Dynamic  
888 Global Vegetation Model, *Global Ecology and Biogeography*, 10, 661-677,  
889 10.1046/j.1466-822X.2001.00175.x, 2001.

890 Tokinaga, H., Xie, S.-P., Deser, C., Kosaka, Y., and Okumura, Y. M.: Slowdown  
891 of the Walker circulation driven by tropical Indo-Pacific warming, *Nature*,  
892 491, 439-443, 2012.

893 Wang, G., and Alo, C. A.: Changes in precipitation seasonality in West Africa  
894 predicted by RegCM3 and the impact of dynamic vegetation feedback,  
895 *International Journal of Geophysics*, 2012, 2012.

896 Wang, G., Eltahir, E., Foley, J., Pollard, D., and Levis, S.: Decadal variability of  
897 rainfall in the Sahel: results from the coupled GENESIS-IBIS atmosphere-  
898 biosphere model, *Climate Dynamics*, 22, 625-637, 2004.

899 Wang, G., and Eltahir, E. A.: Biosphere—atmosphere interactions over West  
900 Africa. II: Multiple climate equilibria, *Quarterly Journal of the Royal*  
901 *Meteorological Society*, 126, 1261-1280, 2000.

902 Wårlind, D., Smith, B., Hickler, T., and Arneth, A.: Nitrogen feedbacks  
903 increase future terrestrial ecosystem carbon uptake in an individual-based  
904 dynamic vegetation model, *Biogeosciences*, 11, 6131-6146, 10.5194/bg-11-  
905 6131-2014, 2014.

906 Weber, U., Jung, M., Reichstein, M., Beer, C., Braakhekke, M., Lehsten, V.,  
907 Ghent, D., Kaduk, J., Viovy, N., and Ciais, P.: The interannual variability of  
908 Africa's ecosystem productivity: a multi-model analysis, *Biogeosciences*, 6,  
909 285-295, 2009.

910 Wramneby, A., Smith, B., and Samuelsson, P.: Hot spots of vegetation-  
911 climate feedbacks under future greenhouse forcing in Europe, *J. Geophys.*  
912 *Res.*, 115, D21119, 10.1029/2010jd014307, 2010.

913 Wu, M., Knorr, W., Thonicke, K., Schurgers, G., Camia, A., and Arneth, A.:  
914 Sensitivity of burned area in Europe to climate change, atmospheric CO<sub>2</sub>  
915 levels and demography: A comparison of two fire - vegetation models,  
916 *Journal of Geophysical Research: Biogeosciences*, 10.1002/2015JG003036,  
917 2015.

918 Xu, Z., Chang, P., Richter, I., and Tang, G.: Diagnosing southeast tropical  
919 Atlantic SST and ocean circulation biases in the CMIP5 ensemble, *Climate*  
920 *dynamics*, 43, 3123-3145, 2014.

921 Young, I.: Seasonal variability of the global ocean wind and wave climate,  
922 *International Journal of Climatology*, 19, 931-950, 1999.

923 Yu, M., Wang, G., and Pal, J. S.: Effects of vegetation feedback on future  
924 climate change over West Africa, *Climate Dynamics*, 1-20, 2015.

925 Zeng, N., Neelin, J. D., Lau, K.-M., and Tucker, C. J.: Enhancement of  
926 interdecadal climate variability in the Sahel by vegetation interaction,  
927 *Science*, 286, 1537-1540, 1999.

928 Zhang, W., Jansson, C., Miller, P., Smith, B., and Samuelsson, P.:  
929 Biogeophysical feedbacks enhance the Arctic terrestrial carbon sink in  
930 regional Earth system dynamics, *Biogeosciences*, 11, 5503-5519, 2014.

931 Zhou, L., Tian, Y., Myneni, R. B., Ciais, P., Saatchi, S., Liu, Y. Y., Piao, S., Chen,  
932 H., Vermote, E. F., Song, C., and Hwang, T.: Widespread decline of Congo  
933 rainforest greenness in the past decade, *Nature*, 509, 86-90,  
934 [10.1038/nature13265](https://doi.org/10.1038/nature13265), 2014.

935 Zhu, Z., Bi, J., Pan, Y., Ganguly, S., Anav, A., Xu, L., Samanta, A., Piao, S.,  
936 Nemani, R. R., and Myneni, R. B.: Global data sets of vegetation leaf area  
937 index (LAI) 3g and Fraction of Photosynthetically Active Radiation (FPAR)  
938 3g derived from Global Inventory Modeling and Mapping Studies (GIMMS)  
939 Normalized Difference Vegetation Index (NDVI3g) for the period 1981 to  
940 2011, *Remote Sensing*, 5, 927-948, 2013.

941

942

943

944

945

946

947

948

949

950

951

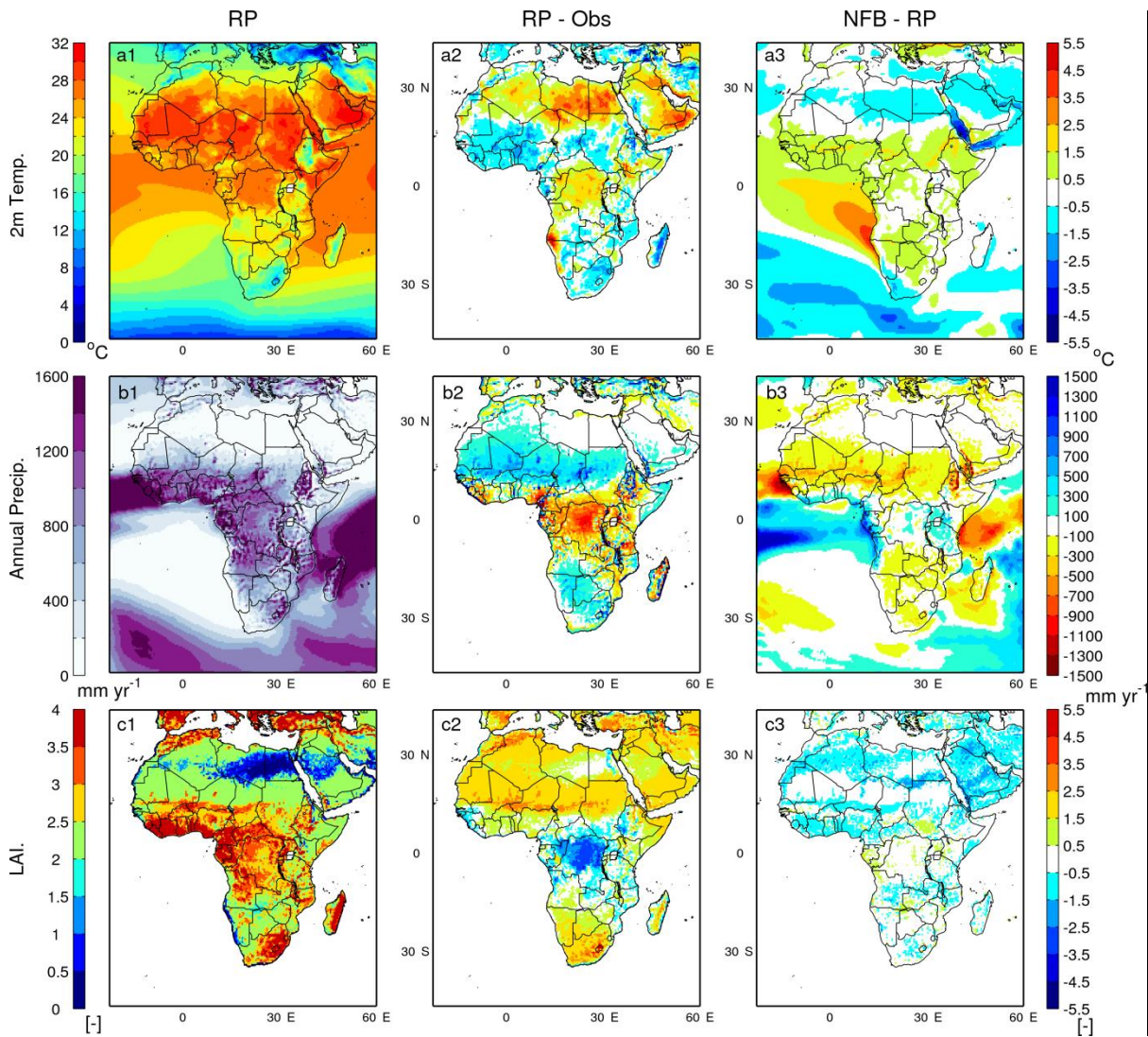
952

953

954

955  
956

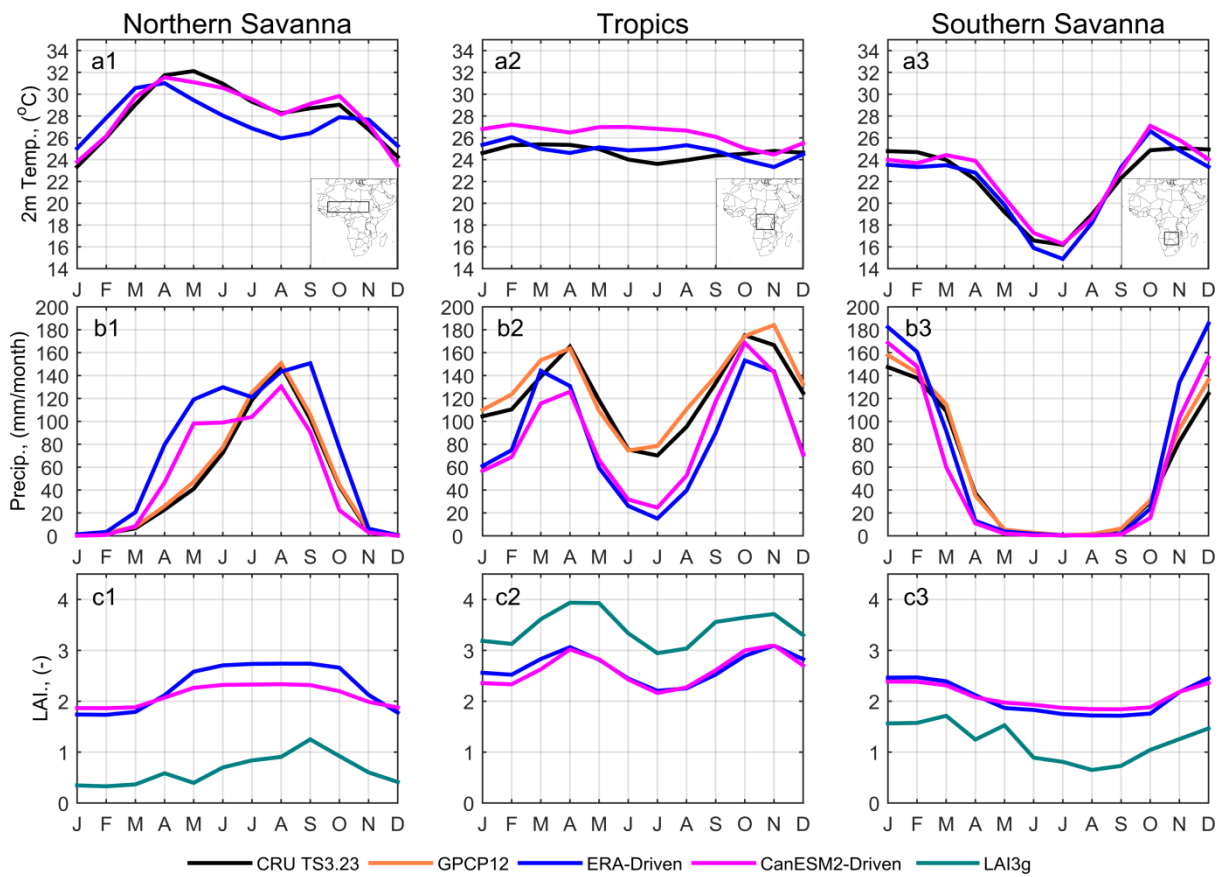
## Figures and Tables



957

958 Fig. 1. Comparison between simulated and observed (a) annual mean near-surface air temperature, (b)  
959 annual precipitation and (c) annual maximum LAI for the period 1997-2010. Variables from the RP experiment  
960 (a1-c1) are compared with observations (a2-c2) and with those from the FB experiment (a3-c3), using RP  
961 minus observation and FB minus RP. For the comparison with observations (a2-c2), we used CRU temperature  
962 (a2) and precipitation (b2), as well as LAI3g (Zhu et al., 2013)(c2).

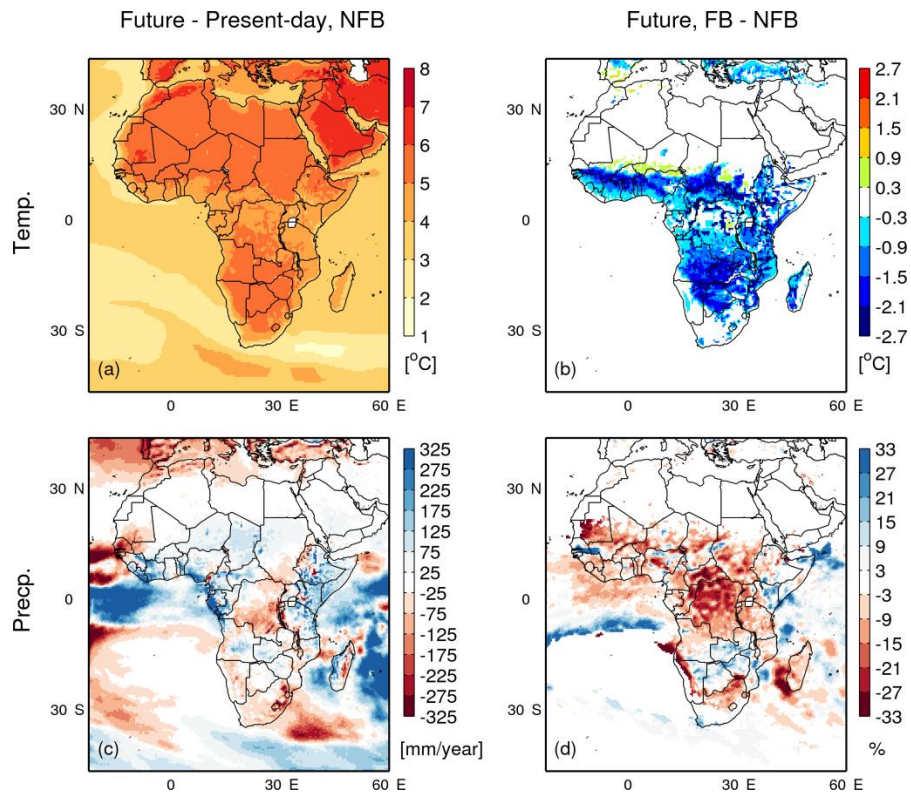




964

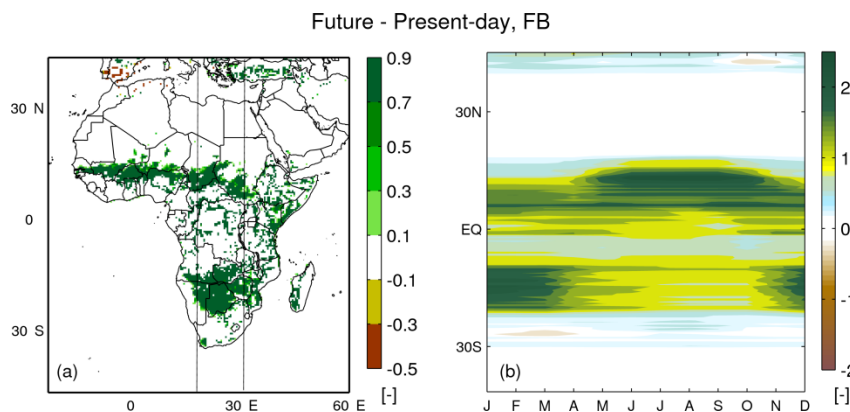
965  
966  
967  
968

Fig. 2. Simulated seasonal cycle and observations for northern savannah (inset in a1), central Africa (inset in a2) and southern savannah (inset in a3) for the period 1997-2010. 2m temperature (a1-a3) and precipitation (b1-b3) are as Fig. 1. For LAI (c1-c3) monthly mean tile-weighted simulated LAI over the averaging period are used to compare with the observation.



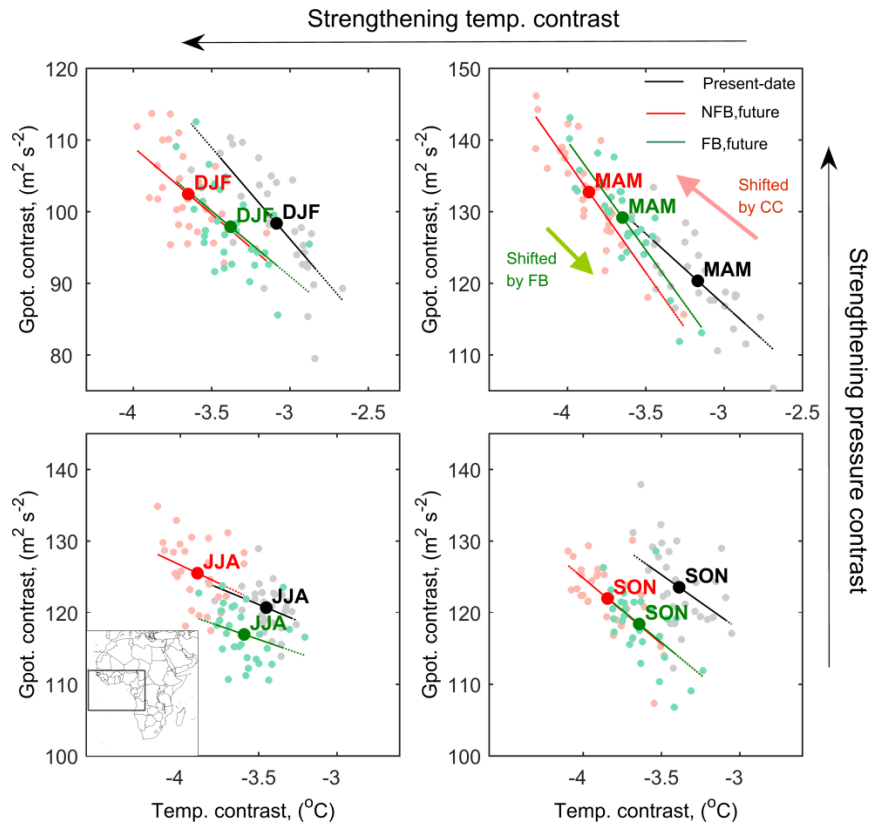
969

970 Fig. 3. Changes in surface temperature and precipitation due to climate change and vegetation feedback.  
 971 The calculation of climate change signal and vegetation feedbacks, present-day and future periods are defined  
 972 in Sect. 2.2. For (d), the percentage is calculated as the difference between FB and NFB (vegetation feedback)  
 973 divided by the present-day level and multiplied by 100. Grid points with annual mean precipitation <20 mm  
 974 year<sup>-1</sup> are skipped.



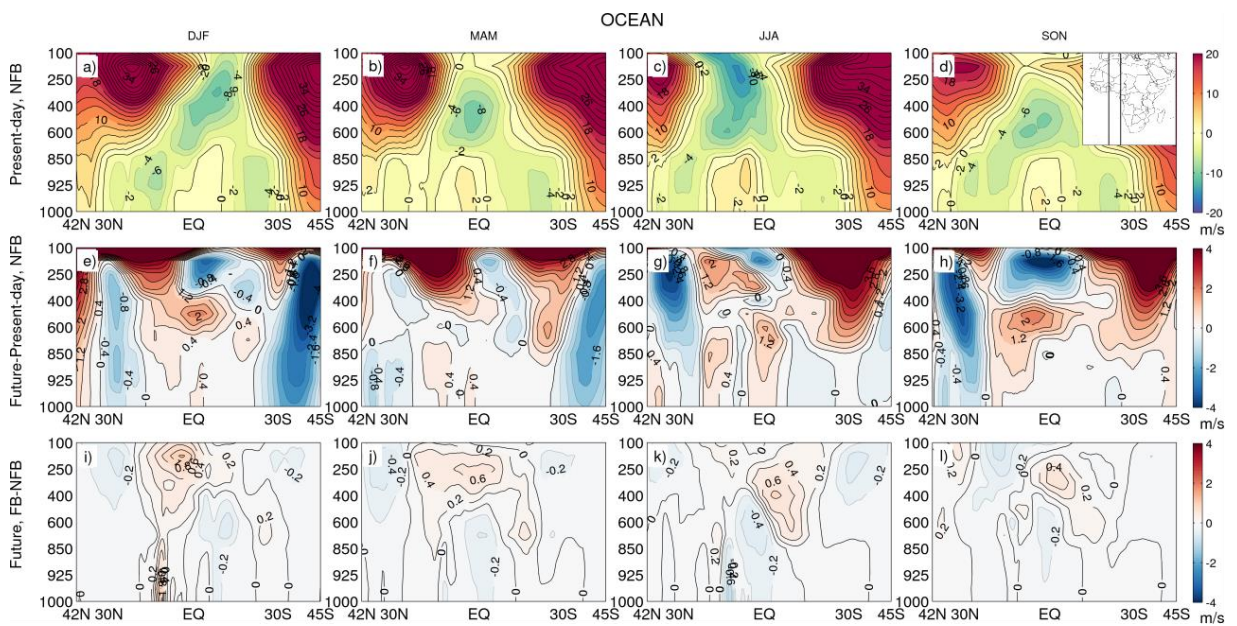
975

976 Fig. 4. (a) Change in forest fraction and (b) seasonal change in zonal mean forest LAI in the longitude band  
 977 between 18°E and 30°E (lines in a), calculated as future minus present-day in FB experiment. Present-day and  
 978 future periods are defined in Sect. 2.2.



979

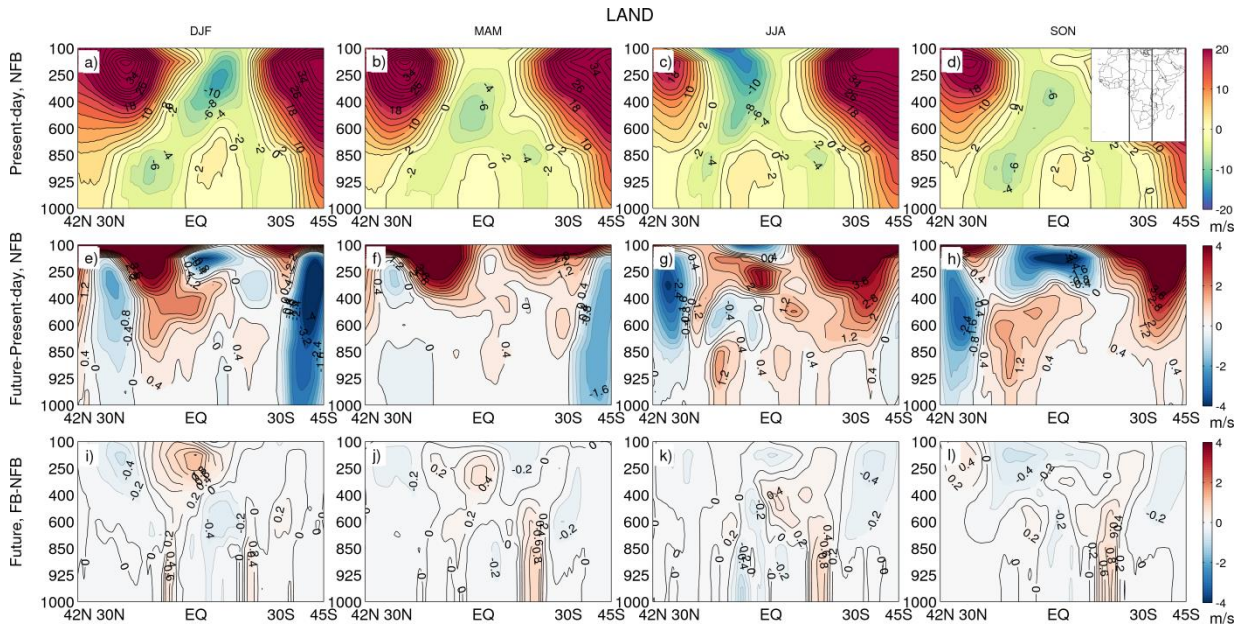
980 Fig. 5. Changes in atmospheric ocean-land temperature contrast ( $\nabla T$ ) and geopotential contrast ( $\nabla \phi$ ),  
 981 represented by the mean contrast at the three pressure levels 850, 925 and 975 hPa (ocean minus land) within  
 982 the domain  $15^{\circ}\text{N}$ - $15^{\circ}\text{S}$ ,  $24^{\circ}\text{W}$ - $20^{\circ}\text{E}$  (see the inset in the panel for JJA), for the NFB and FB simulation in the  
 983 present-day and the future period (as defined in Sect. 2.2). Each scatter point represents the relation between  
 984  $\nabla \phi$  and  $\nabla T$  for the correspondent season of one year, and the slopes represent its sensitivity during the  
 985 selected periods.



986

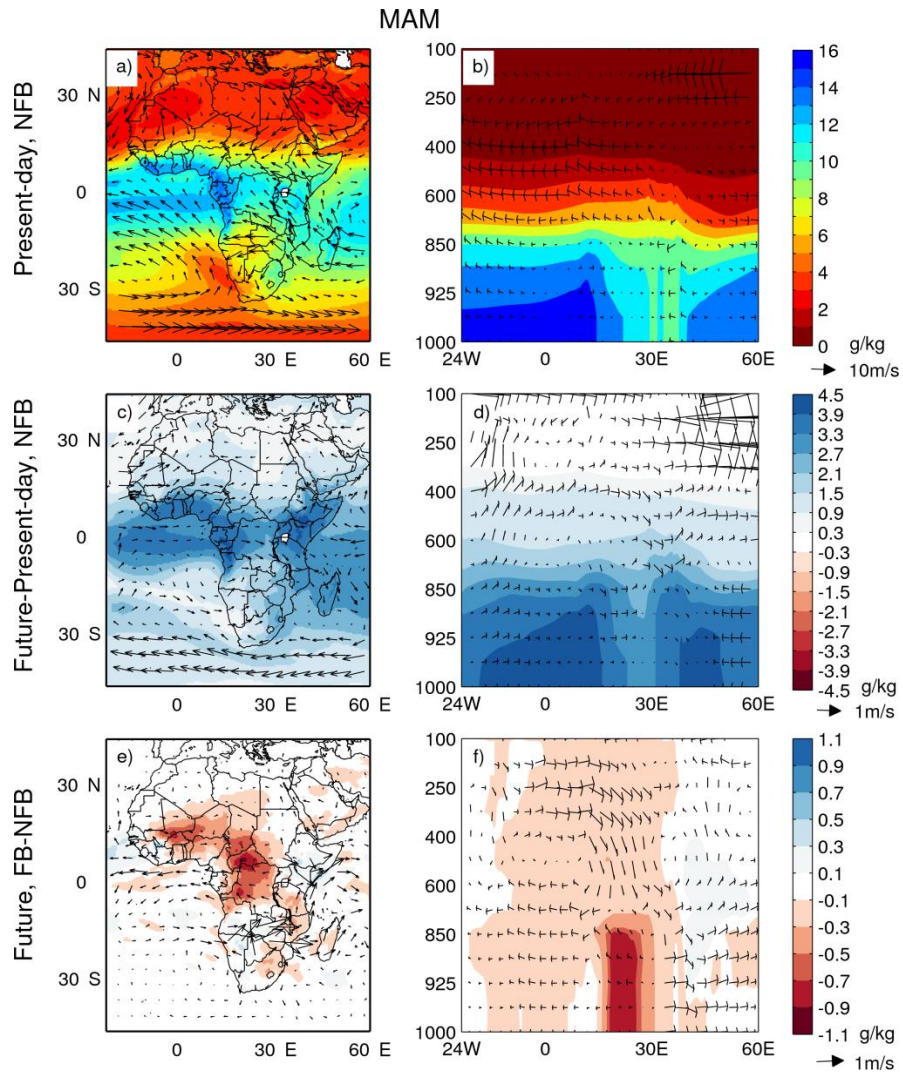
987 Fig. 6. Seasonal mean zonal wind speed in a cross section over adjacent Atlantic ocean ( $0$ - $10^{\circ}\text{E}$ , see the  
 988 inset in d), for present-day (1st row), changes in future (future minus present-day, 2nd row) and the  
 989 differences between FB and NFB runs in future (FB minus NFB, 3rd row). Unit is  $\text{m s}^{-1}$ , positive values represent

990 westerlies and negative values represent easterlies. Present-day and future periods are defined in Sect. 2.2  
 991 Contour intervals from top row to bottom row are  $2\text{m s}^{-1}$ ,  $0.4\text{m s}^{-1}$  and  $0.2\text{m s}^{-1}$ , respectively.



992

993 Fig. 7. As Fig. 6 but for longitudinal band over land ( $10^{\circ}\text{E}-30^{\circ}\text{E}$ , see the inset in d).



994

995 Fig. 8. Atmospheric circulation (arrows,  $\text{m s}^{-1}$ ) and specific humidity (colour contours,  $\text{g kg}^{-1}$ ) at 850 hPa  
 996 pressure level for MAM, displayed as (a, c, e) for the entire domain, and (b, d, f) as a cross section for a latitude  
 997 band between  $2.5^\circ\text{S}$  and  $2.5^\circ\text{N}$ , for present day (top), climate change impacts (middle) and the vegetation  
 998 feedback (bottom). Definitions for calculation period, climate change signal and vegetation feedbacks are  
 999 given in Sect. 2.2.

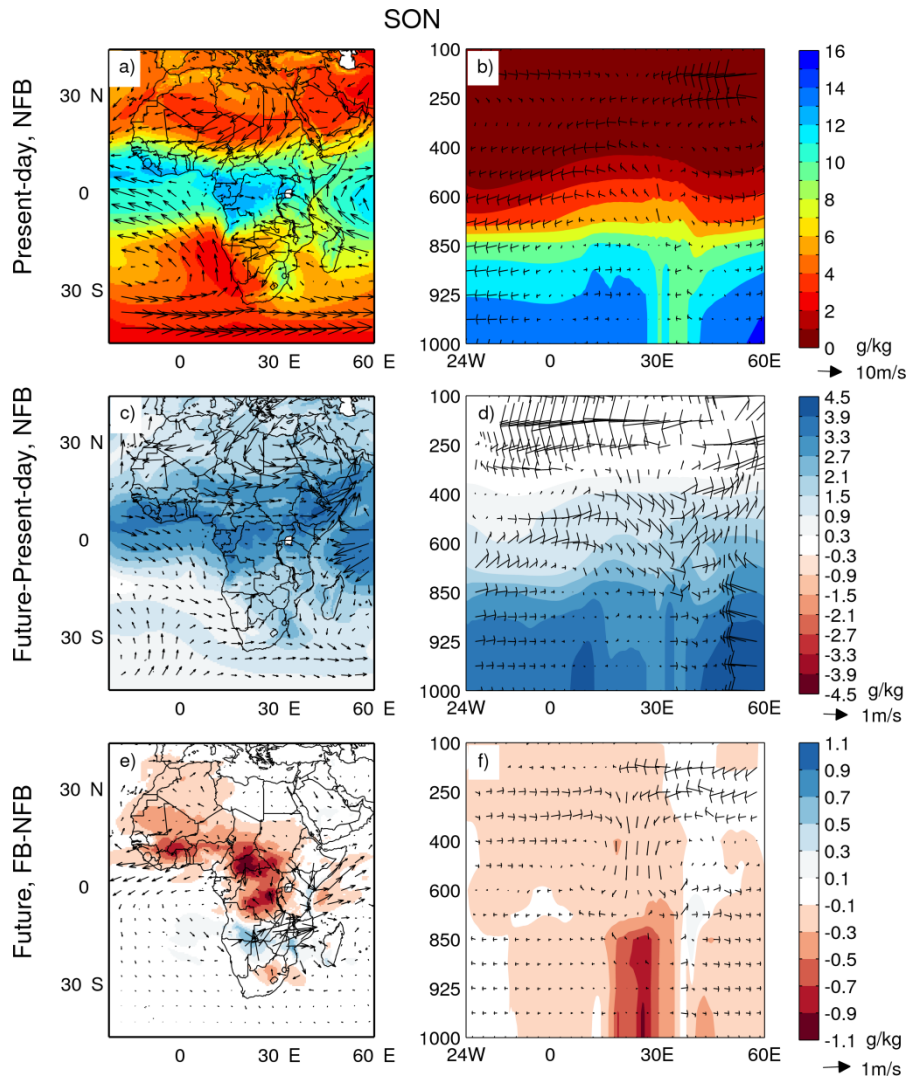


Fig. 9. As Fig. 8 but for SON.

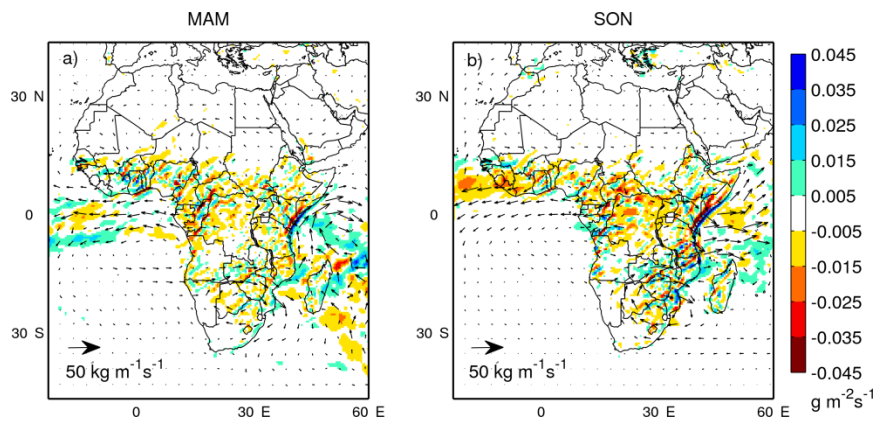
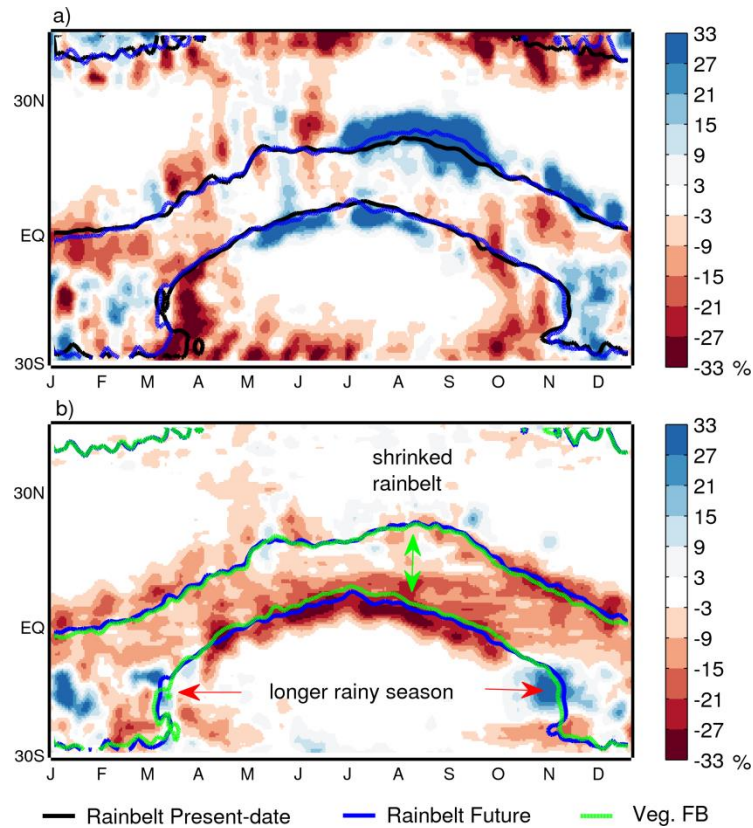


Fig. 10. Changes in vertically integrated moisture flux (arrows,  $\text{kg m}^{-1} \text{s}^{-1}$ ) and moisture flux convergence (colour contours,  $\text{g m}^{-2} \text{s}^{-1}$ ) caused by vegetation feedback, averaged over the future period (as defined in Sect. 2.2) for (a) MAM and (b) SON.



1006

1007 Fig. 11. Daily changes in precipitation averaged over the longitude band 18°E-30°E, represented as relative  
 1008 changes in daily precipitation intensity (shading, %) and rainbelt location (contour) due to (a) climate change  
 1009 and (b) vegetation feedback for future. The rainbelt location is defined as 2mm day<sup>-1</sup> contour. 10-day running  
 1010 mean is applied for daily values.

1011 Table 1. Experimental design for the investigation of the vegetation-climate feedbacks in this study.

Runs	Vegetation Feedbacks	Radiative forcing <sup>a</sup>	CO <sub>2</sub> forcing <sup>b</sup> for vegetation sub-model	Simulated period	Boundary condition
RP	Dynamic	Historical	Historical	1979-2011	ERA-Interim
FB	Dynamic	Transient under RCP8.5	Transient under RCP8.5	1961-2100	CanESM2
NFB	Prescribed vegetation simulated from 1961 to 1990	Transient under RCP8.5	Transient under RCP8.5	1991-2100	CanESM2
FB_CC	Dynamic	Transient under RCP8.5	Historical until 2005 and constant afterward	1991-2100	CanESM2

1012 Notes: a, using equivalent atmospheric CO<sub>2</sub> concentration; b, using actual atmospheric CO<sub>2</sub> concentration.

1013

1014

1015